Universal model of strong coupling at the nonlinear resonance in open cavity-QED systems

Mikhail Tokman,[1] Maria Erukhimova,[1] Qianfan Chen,[2] and Alexey Belyanin[2]
[1]*Institute of Applied Physics, Russian Academy of Sciences, Nizhny Novgorod, 603950, Russia*
[2]*Department of Physics and Astronomy, Texas A&M University, College Station, Texas 77843, USA*

(Received 20 December 2021; accepted 2 May 2022; published 10 May 2022)

Many molecular, quantum-dot, and optomechanical nanocavity-QED systems demonstrate strong nonlinear interactions between electrons, photons, and phonon (vibrational) modes. We show that such systems can be described by a universal model in the vicinity of the nonlinear resonance involving all three degrees of freedom. We solve the nonperturbative quantum dynamics in the strong-coupling regime of the nonlinear resonance, taking into account quantization, dissipation, and fluctuations of all fields. We find analytic solutions for quantum states in the rotating-wave approximation which demonstrate tripartite quantum entanglement once the strong-coupling regime is reached. We show how the strong coupling at the nonlinear resonance modifies photon emission and vibrational spectra, and how the observed spectra can be used to extract information about relaxation rates and the nonlinear coupling strength in specific systems.

DOI: 10.1103/PhysRevA.105.053707

I. INTRODUCTION

Nonlinear optical interactions acquire qualitatively new features in the strong-coupling regime of cavity quantum electrodynamics (QED), especially when utilizing an extreme field localization achievable in nanophotonic cavities. Even in the standard cavity-QED scenario of the strong coupling at the two-wave resonance between only two degrees of freedom, e.g., between an electronic or vibrational transition in a molecule and an electromagnetic (EM) cavity mode, strong coupling has been shown to modify the properties of Raman scattering, generation of harmonics, four-wave mixing, and nonlinear parametric interactions, with applications in photochemistry, quantum information, and quantum sensing; see, e.g., [1–12].

The dynamics becomes more complicated but also more interesting when the strong-coupling regime is realized at the *nonlinear* resonance between three or more degrees of freedom. One possible example where it can be realized is a molecule or an ensemble of molecules placed in a photonic or plasmonic nanocavity, e.g., [11–18]. In this case the fermion system may comprise two or more electron states forming an optical transition at frequency ω_e, and the nonlinear parametric process may involve, e.g., a decay of the electron excitation into a cavity photon at frequency ω and a phonon of a given vibrational mode of a molecule at frequency Ω, under the nonlinear resonance condition $\omega_e = \omega + \Omega$, or an absorption of a photon with simultaneous creation of electron and phonon excitations, given by the nonlinear resonance condition $\omega = \omega_e + \Omega$. When the strength of such a nonlinear three-wave interaction is higher than the dissipation rates, hybrid electron-photon-phonon states are formed. If the phonon mode is classical, the parametric process is simply the modulation of the electron-photon coupling by molecular vibrations which serve as an external driving force for the electron-photon quantum dynamics. If the phonon mode is quantized, the strong coupling between photon, phonon, and electron degrees of freedom near the nonlinear resonance $\omega_e = \omega \pm \Omega$ leads inevitably to the formation of tripartite entangled states belonging to the family of Greenberger-Horne-Zeilinger (GHZ) states [19].

Another route to the nonlinear resonance is within the framework of cavity optomechanics, e.g. [20–25], and quantum acoustics [26–28]. It can occur in the situations where mechanical oscillations of a cavity parameter at frequency Ω modulate the frequency of the photon cavity mode. Here again the nonlinear resonance $\omega_e = \omega \pm \Omega$ at strong coupling should give rise to tripartite entangled states of the electrons, photons, and mechanical vibrations [29]. While quantization of all three degrees of freedom in experiment remains an unsolved challenge, strong coupling and entanglement of acoustic phonons [30,31], resolving the energy levels of a nanomechanical oscillator [28], or cooling a macroscopic system into its motional ground state [32] have already been demonstrated.

Yet another situation leading to the nonlinear resonance is when the phonons or molecular vibrations modulate the electron transition frequency. This coupling is typically introduced via the Huang-Rhys theory; see the Hamiltonian (14) below. The same type of the Hamiltonian is often used to describe the effect of phonons on the coupling of a quantum dot or an optically active defect in a solid matrix to the EM cavity field [33–37]. The exciton-photon coupling strength (Rabi frequency) in nanocavities can be even high enough to exceed the phonon frequency, which brings the system to the ultrastrong-coupling regime with respect to the phonon mode [37].

There are a great variety of models and formalisms describing these diverse physical systems, and attempts have been made to establish connections between different models.

For example, it was shown in [24] that plasmon-enhanced Raman scattering on individual molecules can be mapped onto a cavity optomechanics Hamiltonian when the plasmon frequency is far detuned from the electronic transition in a molecule, i.e., no electrons are excited. In this case the vibrational mode of a molecule is analogous to the mechanical oscillations of a cavity parameter. In [3] it was argued that Stokes Raman scattering in molecules under the condition of a strong coupling between the vibrational mode and the cavity mode is equivalent to the parametric decay of the pump photon into the Stokes photon and the vibrational quantum. In both cases, a simple linear resonance $\omega = \Omega$ was assumed and the EM field was far detuned from any electronic transition in a molecule, thus excluding any real electron excitation. In [12] resonant Raman scattering of single molecules when the two-wave exciton-photon coupling frequency is comparable to the vibrational frequency was analyzed. The situation when the Rabi frequency becomes comparable to the vibrational frequency was also considered in [19].

In this paper we deal with the strong coupling at the nonlinear three-wave resonance $\omega_e = \omega \pm \Omega$ when the excitation of the electron transition and energy exchange between all three degrees of freedom are of principal importance. We show that in the rotating-wave approximation (RWA) (i.e., excluding ultrastrong-coupling regimes) all physical models of electron-photon-vibrational coupling in molecular, optomechanical, and any other coupled three-mode system can be mapped onto the universal "parametric" Hamiltonian, independently on the specific physical mechanism of coupling. This result is surprising as the original Hamiltonians describing these systems have a very different structure; see the next section.

We call this Hamiltonian "parametric" for lack of a better word because it resembles the structure of the Hamiltonian describing spontaneous parametric down-conversion of a pump photon field into signal and idler photons, assuming that all three fields are quantized [38]. However, one should keep in mind that in our case one of the degrees of freedom is fermionic (quantum emitter) and we are interested in the nonperturbative regime of strong coupling when the excitation of the quantum emitter is not small. This is the regime most interesting for quantum technology applications as it actively involves the fermionic qubit in the processes of writing, reading, and transferring the information encoded in a quantum state.

Note that the system *must* be in the RWA regime for the nonlinear resonance and all associated physics to exist and make sense. Otherwise, the three-wave and two-way resonances overlap [19] and the GHZ-like entangled states cannot be created. Also, it becomes impossible to build a universal Hamiltonian. That is why the ultrastrong-coupling regimes are not of interest to us in this paper.

When solving for the quantum dynamics of the resulting nonlinear coupled system, we include the effects of decoherence and coupling of each dynamic subsystem (electrons, photons, and phonons) to its own reservoir in the Markov approximation. Previous works (see, e.g., [35,37]) included the non-Markovian effects in the coupling of the two-wave exciton-photon resonance to the phonon reservoir. In our case the phonon mode, which is strongly coupled to the exciton and photon modes through the nonlinear resonance, is part of the dynamical system. One could say that the phonon effect on the dynamics is "extremely non-Markovian," except that this terminology ceases to have any meaning in this case. The Markov approximation is of course related only to (weak) coupling of all components of the dynamic system to their dissipative reservoirs.

Within the formalism of the stochastic equation of evolution for the state vector we are able to find the general analytic solution for the nonperturbative dynamics of the open quantum system. This approach is well known [39], but it is usually applied for numerical Monte Carlo simulations [40–48]. We recently developed a version of stochastic Schrödinger equation suitable for analytic solutions in open strongly coupled cavity-QED problems [19,49]. We calculate the photon and phonon emission spectra to obtain the experimentally observable signatures of the strong-coupling regime and tripartite quantum entanglement.

The effect of the phonon reservoir leads to qualitatively new features in both photon and phonon emission spectra at the nonlinear resonance that are not present in the standard Rabi oscillations regime and were not found in our recent work [19]. In particular, the intermediate relaxation pathways result in a richer multipeak structure. Since we are able to find analytic solutions for the quantum dynamics in systems of coupled electron, photon, and phonon excitations including dissipation and fluctuation effects in all subsystems, we can retrieve all experimental parameters from the relative amplitudes and positions of the spectral peaks, namely, transition energies and frequencies, matrix elements of the optical transitions, the spatial structure of the field modes, relaxation rates for all constituent subsystems, ambient temperatures, etc. We believe that the results obtained in this paper will be useful for designing and interpreting the experiments on a broad range of cavity-QED systems.

The paper is structured as follows. In Sec. II we present the Hamiltonian for coupled quantized fermion, photon, and phonon fields near the nonlinear resonance for one particular mechanism of three-wave coupling. In Sec. III we show that a large variety of different three-wave coupling mechanisms and physical systems are reduced to the same Hamiltonian which therefore can serve as a universal model of the strongly coupled nonlinear resonance. Section IV includes the effects of dissipation, decoherence, and fluctuations within the stochastic equation for the state vector which describes the evolution of an open system in contact with dissipative reservoirs. As compared to our recent work [19,49], we develop a model of fluctuations and dissipative processes which includes all effects of phonon dissipation on the dynamics of the parametric process and the emission spectra. In Sec. V we describe the formation of entangled electron-photon-phonon states for an open system. Section VI calculates the emission spectra of photons and phonons resulting from the nonlinear parametric decay of an electron excitation. Appendixes A and B contain the derivation details.

II. UNIVERSAL HAMILTONIAN OF THE NONLINEAR RESONANCE

Consider a simple model of three interacting quantum subsystems which includes (1) an electron transition in a quantum

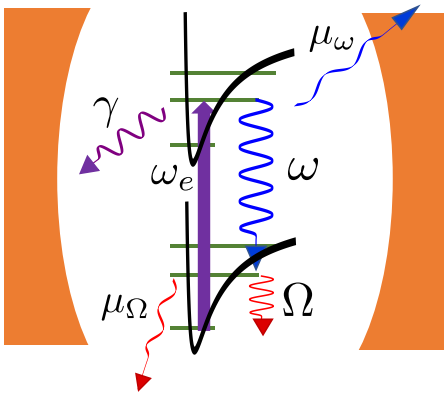

FIG. 1. A sketch of nonlinear resonance for a molecule in a cavity showing the decay of the electron excitation at frequency ω_e into a cavity mode photon at frequency ω and a phonon of a given vibrational mode at frequency Ω. The relaxation rates of the electron, photon, and vibrational excitations are γ, μ_ω, and μ_Ω, respectively.

emitter such as an atom, molecule, optically active impurity, quantum dot, etc., which we will model as a two-level system, (2) a single-mode electromagnetic (EM) field in a cavity, and (3) a mode of mechanical, acoustic, or molecular vibrations ("phonons"). Although in this section we write the Hamiltonian for a specific model, in the next section we show that the same Hamiltonian describes the nonlinear parametric coupling in a variety of physical systems.

The generalization to many bosonic modes or fermionic degrees of freedom is straightforward and still allows analytic solution within the rotating-wave approximation (RWA), but it leads to more cumbersome algebra (see, e.g., [50]), so we will keep only three degrees of freedom for clarity.

Figure 1 shows a generic model of parametric decay of an electron excitation in a quantum emitter (e.g., a molecule) into a photon of a cavity mode at frequency ω and a phonon of a given vibrational mode at frequency Ω, under the condition of the nonlinear resonance $\omega_e \approx \omega + \Omega$.

In the absence of coupling, the partial Hamiltonians are as follows.

A. Two-level fermion system

It is described by a standard effective Hamiltonian

$$\hat{H}_e = \hbar\omega_e \hat{\sigma}^\dagger \hat{\sigma}. \tag{1}$$

Here $\hat{\sigma} = |0\rangle\langle 1|$, $\hat{\sigma}^\dagger = |1\rangle\langle 0|$; $|0\rangle$ and $|1\rangle$ are the eigenstates of an "atom" with energies 0 and $\hbar\omega_e$, respectively. The Hamiltonian Eq. (1) corresponds to the dipole moment operator

$$\hat{\mathbf{d}} = \mathbf{d}(\hat{\sigma}^\dagger + \hat{\sigma}), \tag{2}$$

where $\mathbf{d} = -\mathbf{e}\langle 1|\mathbf{r}|0\rangle$, and $\mathbf{r}$ is a coordinate for the finite motion of a bound electron.

B. EM field

Here we consider a single-mode EM field for simplicity, although including many bosonic field modes does not present any principal difficulties. Besides, in a microcavity or nanocavity other EM modes will be far detuned from the nonlinear resonance. The Hamiltonian is

$$\hat{H}_{em} = \hbar\omega \hat{c}^\dagger \hat{c}. \tag{3}$$

Here $\hat{c}$ and $\hat{c}^\dagger$ are standard bosonic annihilation and creation operators of photons or plasmons in the EM mode of frequency ω. The electric field operator is

$$\hat{\mathbf{E}} = \mathbf{E}(\mathbf{r})\hat{c} + \mathbf{E}^*(\mathbf{r})\hat{c}^\dagger. \tag{4}$$

The spatial structure of the normalization amplitude of the field $\mathbf{E}(\mathbf{r})$ is determined by solving the boundary value problem. The normalization condition is

$$\int_V \frac{\partial[\omega^2\varepsilon(\omega,\mathbf{r})]}{\omega\partial\omega}\mathbf{E}^*(\mathbf{r})\mathbf{E}(\mathbf{r})d^3r = 4\pi\hbar\omega. \tag{5}$$

Here V is the quantization volume, and $\varepsilon(\omega,\mathbf{r})$ the dielectric function of the dispersive medium which fills in the resonator. Equation (5) is derived, e.g., in [51–54].

C. Phonons

We again assume a single bosonic mode of a vibrational field for the same reasons,

$$\hat{H}_p = \hbar\Omega \hat{b}^\dagger \hat{b}, \tag{6}$$

where $\hat{b}$ and $\hat{b}^\dagger$ are phonon annihilation and creation operators. Depending on the situation, they may define, e.g., the radius vector of oscillations of the center of mass of an atom [5,19,55] or a geometric parameter of the optomechanical cavity [22,24],

$$\hat{\mathbf{R}} = \mathbf{Q}\hat{b} + \mathbf{Q}^*\hat{b}^\dagger. \tag{7}$$

The normalization amplitude $\mathbf{Q}$ depends on the system; its absolute value can be expressed through an effective mass of the quantum mechanical oscillator [22]: $|\mathbf{Q}|^2 = \frac{\hbar}{2m_{\text{eff}}\Omega}$.

D. Coupling

The coupling between subsystems is strongest at resonance. Since usually $\omega, \omega_e \gg \Omega$, the two most relevant resonances are a two-wave resonance

$$\omega_e \approx \omega \tag{8}$$

and a three-wave (nonlinear) resonance

$$\omega_e \approx \omega \pm \Omega. \tag{9}$$

There could be also resonances at the harmonics of the phonon frequency: $\omega_e \approx \omega \pm M\Omega$, where M is integer. The modulation of the system parameters by a classical phonon field at frequency Ω was studied, e.g., in [49], and we do not consider the classical field here.

The two-wave resonance in the RWA [40] is described by the Jaynes-Cummings (JC) Hamiltonian [56]

$$\hat{H} = \hbar\omega\hat{c}^\dagger\hat{c} + \hbar\omega_e\hat{\sigma}^\dagger\hat{\sigma} + \hbar\left(\Omega_R^{(2)}\hat{\sigma}^\dagger\hat{c} + \text{H.c.}\right). \tag{10}$$

The electric dipole coupling between the electron and EM subsystems is expressed here through the effective Rabi frequency for the two-wave coupling $\Omega_R^{(2)} = -\frac{\mathbf{d}\cdot\mathbf{E}(\mathbf{r}_0)}{\hbar}$, where $\mathbf{r}_0$ is the coordinate of a pointlike atom.

A three-wave (parametric) resonance appears in many different scenarios. As we show in the next section, various models existing in the literature can be described with one universal Hamiltonian. One of the scenarios leading to the universal three-wave coupling Hamiltonian is when a quantized phonon (vibrational) mode modulates the coupling strength between the electron transition and the EM field mode. In this case the JC Hamiltonian is generalized to the following form [3,19]:

$$\hat{H} = \hbar\omega\hat{c}^\dagger\hat{c} + \hbar\omega_e\hat{\sigma}^\dagger\hat{\sigma} + \hbar\Omega\hat{b}^\dagger\hat{b} + \hbar\big(\Omega_R^{(3)}\hat{\sigma}^\dagger\hat{c}\hat{b} + \text{H.c.}\big), \tag{11}$$

where $\Omega_R^{(3)}$ is the coupling parameter for the three-wave resonance, which depends on the specific coupling mechanism. The above interaction term is written for the decay of an electron transition into the photon and the phonon, i.e., assuming that the electron excitation energy is the largest of the three. This decay process corresponds to the upper (plus) sign in the resonant condition Eq. (9). If we choose the lower (minus) sign in Eq. (9), the three-wave coupling Hamiltonian will become $\hbar(\Omega_R^{(3)}\hat{c}^\dagger\hat{b}\hat{\sigma} + \text{H.c.})$.

Note that the three-wave coupling term in Eq. (11) has the structure formally equivalent to the parametric down-conversion (PDC) Hamiltonian describing the parametric decay of the quantized pump field into quantized signal and idler modes [38,57]. Of course, one difference is that all fields in the photonic PDC process are described by bosonic operators whereas the electron excitation in Eq. (11) is described by fermionic operators, giving rise to its specific nonlinearities.

The strong-coupling regime at the nonlinear resonance is realized when the three-wave coupling parameter in Eq. (11) is larger than a certain combination of the relaxation constants $\gamma, \mu_\omega, \mu_\Omega$ of all subsystems. The exact criterion can be retrieved from the analytic solution presented in Secs. V and VI below.

The specific form of the parameter $\Omega_R^{(3)}$ depends on the nonlinear coupling mechanism. For example, a phonon mode can modulate the position of the center of mass of an "atom" within a spatially nonuniform distribution of the EM field of a cavity mode. It can be realized for all kinds of quantum emitters: an electron transition in a molecule, a quantum dot or defect in a solid matrix, an optomechanical system with a varying cavity parameter, etc. In this case, in the limit of a small amplitude of vibrations, one can obtain that [19]

$$\Omega_R^{(3)} = -\frac{1}{\hbar}[\mathbf{d}(\mathbf{Q}\cdot\nabla)\mathbf{E}]_{\mathbf{r}=\mathbf{r}_0}. \tag{12}$$

The Hamiltonian in Eq. (11) is valid if the three-wave resonance is well separated from the two-wave one. The conditions for that are [19]

$$|\omega_e - \omega - \Omega| \ll |\omega_e - \omega|, \ \left|\Omega_R^{(2,3)}\right| \ll \Omega. \tag{13}$$

In the next section we will see that if the conditions Eq. (13) are satisfied, other models of three-wave coupling can be reduced to the universal parametric Hamiltonian Eq. (11). Note that in plasmonic nanocavities the two-wave or/and three-wave Rabi frequency $\Omega_R^{(2,3)}$ can become higher than the vibrational or phonon frequency Ω, which would violate the last of inequalities Eq. (13); see [12,19,37].

III. THE MODELS DESCRIBED BY THE UNIVERSAL PARAMETRIC HAMILTONIAN

In addition to the three-wave coupling mechanism considered in the previous section, there are other ways for phonons or any mechanical oscillations to affect the coupling between the EM cavity field and the quantum emitter. Here we give several examples, assuming without loss of generality that the amplitudes $\mathbf{Q}$ in the expression for the position displacement operator in Eq. (7) are real functions.

A. Phonons modulate the energy of the electron transition

For a single-phonon mode the Hamiltonian is

$$\hat{H} = \hbar\omega\hat{c}^\dagger\hat{c} + \hbar\omega_e\hat{\sigma}^\dagger\hat{\sigma} + \hbar\Omega\hat{b}^\dagger\hat{b} + \hbar\big(\Omega_R^{(2)}\hat{\sigma}^\dagger\hat{c} + \text{H.c.}\big) + \hbar\sqrt{S}\Omega\hat{\sigma}^\dagger\hat{\sigma}(\hat{b} + \hat{b}^\dagger). \tag{14}$$

Here S is the Huang-Rhys factor, which determines the dependence of the transition energy on the dimensionless amplitude $\hat{b} + \hat{b}^\dagger$ of the phonon oscillations. There are numerous studies of this type of modulation; see, e.g., [5,12–15,55,58] and references therein. The same type of coupling is also used in a Holstein-Tavis-Cummings model, e.g., [59–61]. Let us call Eq. (14) the "molecular" Hamiltonian, although it also describes the exciton-phonon coupling in quantum-dot systems [34–37].

B. Phonons modulate some geometric parameter of the cavity

This type of coupling is usually described by the Hamiltonian of the type

$$\hat{H} = \hbar\omega\hat{c}^\dagger\hat{c} + \hbar\omega_e\hat{\sigma}^\dagger\hat{\sigma} + \hbar\Omega\hat{b}^\dagger\hat{b} + \hbar\big(\Omega_R^{(2)}\hat{\sigma}^\dagger\hat{c} + \text{H.c.}\big) - \hbar g\hat{c}^\dagger\hat{c}(\hat{b} + \hat{b}^\dagger) \tag{15}$$

or its multimode extension. Here the factor g determines the linear dependence of the resonant frequency of the cavity on some geometric parameter $\mathbf{G}$ modulated by mechanical vibrations:

$$g = -\mathbf{Q}\frac{\partial\omega}{\partial\mathbf{G}}.$$

There are numerous studies of this model as well; see, e.g., [21–24] for examples of classical and recent papers, reviews, and numerous references therein. We will call Eq. (15) the "optomechanical" Hamiltonian.

The Hamiltonians Eq. (14) and (15) appear to be very different from Eq. (11). Indeed, they both contain the standard two-wave resonance as opposed to Eq. (11) and their three-wave coupling terms are completely different. Moreover, the nonlinear coupling in Eq. (15) does not even involve the fermionic degree of freedom. Nevertheless, we will show that when the conditions Eq. (13) are satisfied, the "molecular" and "optomechanical" Hamiltonians are equivalent to the universal Hamiltonian in Eq. (11).

To prove this statement, we write the Hamiltonian Eq. (11) in the interaction representation

$$\hat{H}_{\text{int}} = e^{i\hat{H}_0 t}\hat{V}e^{-i\hat{H}_0 t}, \tag{16}$$

where

$$\hat{H}_0 = \hbar\omega\hat{c}^\dagger\hat{c} + \hbar\omega_e\hat{\sigma}^\dagger\hat{\sigma} + \hbar\Omega\hat{b}^\dagger\hat{b}, \quad \hat{V} = \hbar\big(\Omega_R^{(3)}\hat{\sigma}^\dagger\hat{c}\hat{b} + \text{H.c.}\big).$$

This yields

$$\hat{H}_{\rm int} = \hbar\big(\Omega_R^{(3)}\hat{\sigma}^\dagger\hat{c}\hat{b}e^{i(\omega_e-\omega-\Omega)t} + \text{H.c.}\big). \tag{17}$$

Next, we write the Hamiltonians in Eqs. (14) and (15) in the interaction representation by defining the unperturbed Hamiltonian as

$$\hat{H}_0 = \hbar\omega\hat{c}^\dagger\hat{c} + \hbar\omega_e\hat{\sigma}^\dagger\hat{\sigma} + \hbar\Omega\hat{b}^\dagger\hat{b} + \hbar\big(\Omega_R^{(2)}\hat{\sigma}^\dagger\hat{c} + \text{H.c.}\big). \tag{18}$$

This gives

$$\hat{V} = \hat{V}_{\rm mol} = \hbar\sqrt{S}\Omega\hat{\sigma}^\dagger\hat{\sigma}(\hat{b} + \hat{b}^\dagger) \tag{19}$$

for the "molecular" Hamiltonian and

$$\hat{V} = \hat{V}_{\rm optom} = -\hbar g\hat{c}^\dagger\hat{c}(\hat{b} + \hat{b}^\dagger) \tag{20}$$

for the optomechanical one.

The operator $\hat{H}_0$ given by Eq. (18) is not diagonal. In this case one should generally diagonalize $\hat{H}_0$. However, sometimes a slightly different approach is simpler. Indeed, consider the Hamiltonian given by

$$\hat{H} = \hat{H}_0(\hat{A}_1, \ldots, \hat{A}_N) + \hat{V}(\hat{A}_1, \ldots, \hat{A}_N), \tag{21}$$

where $\hat{A}_i$ are certain operators related to coupled subsystems (here we assume that Hermitian conjugated operators are assigned different numbers "i"). For any interaction operator $\hat{V}$, which can be expanded in a series

$$\hat{V} = \sum_j k_j \prod_{i=1}^{N_j} (\hat{A}_i)^{n_{ji}}$$

(here n_{ji} are positive integers), the following relationships are true:

$$\begin{aligned}\hat{H}_{\rm int} &= e^{i\hat{H}_0 t}\hat{V}(\hat{A}_1, \ldots, \hat{A}_N)e^{-i\hat{H}_0 t} \\ &= \sum_j k_j \prod_{i=1}^{N_j} e^{i\hat{H}_0 t}(\hat{A}_i)^{n_{ji}}e^{-i\hat{H}_0 t} \\ &= \sum_j k_j \prod_{i=1}^{N_j} (e^{i\hat{H}_0 t}\hat{A}_i e^{-i\hat{H}_0 t})^{n_{ji}},\end{aligned}$$

from which one obtains

$$\hat{H}_{\rm int} = \hat{V}(\widehat{\tilde{A}}_1, \ldots, \widehat{\tilde{A}}_N), \tag{22}$$

where

$$\widehat{\tilde{A}}_i(t, \hat{A}_1, \ldots, \hat{A}_N) = e^{i\hat{H}_0 t}\hat{A}_i e^{-i\hat{H}_0 t}. \tag{23}$$

The operators $\widehat{\tilde{A}}_i$ satisfy the Heisenberg equations

$$\frac{\partial\widehat{\tilde{A}}_i}{\partial t} = \frac{i}{\hbar}[\hat{H}_0, \widehat{\tilde{A}}_i] \tag{24}$$

for the initial conditions $\widehat{\tilde{A}}_i(t=0) = \hat{A}_i$. In particular, for the Hamiltonian $\hat{H}_0$ given by Eq. (18) one obtains

$$\frac{\partial\widehat{\tilde{\sigma}}}{\partial t} = -i\omega_e\widehat{\tilde{\sigma}} - i\Omega_R^{(2)}\widehat{\tilde{c}}(1 - 2\widehat{\tilde{\sigma}}^\dagger\widehat{\tilde{\sigma}}), \tag{25}$$

$$\frac{\partial\widehat{\tilde{c}}}{\partial t} = -i\omega\widehat{\tilde{c}} - i\Omega_R^{(2)*}\widehat{\tilde{\sigma}}, \tag{26}$$

where we used the integral of motion $\widehat{\tilde{\sigma}}^\dagger\widehat{\tilde{\sigma}} + \widehat{\tilde{\sigma}}\widehat{\tilde{\sigma}}^\dagger = 1$. Taking into account the condition $|\Omega_R^{(2)}| \ll |\omega_e - \omega|$ which follows from Eqs. (13), when solving for the operators $\widehat{\tilde{c}}$ and $\widehat{\tilde{\sigma}}$ one can neglect the terms of the order of $|\frac{\Omega_R^{(2)}}{\omega_e-\omega}|^2$. For the initial conditions $\widehat{\tilde{\sigma}}\ (t=0) = \hat{\sigma}$ and $\widehat{\tilde{c}}(t=0) = \hat{c}$ the solution expanded in series in powers of the small parameter $|\frac{\Omega_R^{(2)}}{\omega_e-\omega}|$ takes the form

$$\begin{pmatrix}\widehat{\tilde{\sigma}}\\ \widehat{\tilde{c}}\end{pmatrix} = \widehat{\tilde{M}}\begin{pmatrix}\hat{\sigma}\\ \hat{c}\end{pmatrix}, \tag{27}$$

where

$$\widehat{\tilde{M}} = \begin{pmatrix}e^{-i\omega_e t} & 0\\ 0 & e^{-i\omega t}\end{pmatrix} - \begin{pmatrix}0 & \frac{\Omega_R^{(2)}}{\omega_e-\omega}(1 - 2\hat{\sigma}^\dagger\hat{\sigma})(e^{-i\omega t} - e^{-i\omega_e t})\\ \frac{\Omega_R^{(2)*}}{\omega_e-\omega}(e^{-i\omega t} - e^{-i\omega_e t}) & 0\end{pmatrix} + o\left(\left|\frac{\Omega_R^{(2)}}{\omega_e - \omega}\right|^2\right). \tag{28}$$

There is an exact solution for the operator $\widehat{\tilde{b}}$:

$$\widehat{\tilde{b}} = e^{i\hat{H}_0 t}\hat{b}e^{-i\hat{H}_0 t} = \hat{b}e^{-i\Omega t}. \tag{29}$$

Now we substitute the three-wave coupling Hamiltonian Eq. (19) into Eq. (22) and use Eqs. (27)–(29). The conditions Eq. (13) combined with the RWA allow one to keep only slowly varying terms $\propto e^{i(\omega_e-\omega-\Omega)t}$ in the final expression. Taking into account that $\hat{\sigma}^\dagger\hat{\sigma}^\dagger = \hat{\sigma}\hat{\sigma} = 0$ and taking $\frac{1}{\omega_e-\omega} \approx \frac{1}{\Omega}$ in Eq. (28), we obtain the following expression for the "molecular" Hamiltonian in the interaction picture:

$$(\hat{H}_{\rm int})_{\rm mol} = -\hbar\big(\sqrt{S}\Omega_R^{(2)}\hat{\sigma}^\dagger\hat{c}\hat{b}e^{i(\omega_e-\omega-\Omega)t} + \text{H.c.}\big). \tag{30}$$

A similar derivation for the "optomechanical" Hamiltonian given by Eq. (20) leads to the following result:

$$(\hat{H}_{\rm int})_{\rm optom} = -\hbar\left(\frac{g\Omega_R^{(2)}}{\Omega}\hat{\sigma}^\dagger\hat{c}\hat{b}e^{i(\omega_e-\omega-\Omega)t} + \text{H.c.}\right). \tag{31}$$

Clearly, in both cases the Hamiltonian has the same structure as the parametric Hamiltonian Eq. (17), in which

$$\big(\Omega_R^{(3)}\big)_{\rm mol} = -\sqrt{S}\Omega_R^{(2)} \quad \text{or} \quad \big(\Omega_R^{(3)}\big)_{\rm optom} = -\frac{g}{\Omega}\Omega_R^{(2)}. \tag{32}$$

Therefore, one can use the universal parametric Hamiltonian Eq. (11) for all kinds of three-wave couplings after choosing an appropriate expression for the coupling parameter $\Omega_R^{(3)}$.

We emphasize again that the universal character of the parametric Hamiltonian Eq. (11) holds as long as inequalities Eq. (13) are satisfied, which ensure that the three-wave nonlinear resonance can be separated from the two-wave resonance. The structure of the nonlinear coupling term in Eq. (11) could be expected if all three modes are bosonic fields, as in spontaneous parametric down-conversion process. However, the fact that the same Hamiltonian can be extended to two-level (fermionic) transitions with their specific nonlinearity dictated by the Pauli principle is unusual and unexpected.

IV. INCLUDING DISSIPATION AND FLUCTUATIONS WITHIN THE STOCHASTIC EQUATION FOR THE STATE VECTOR

A. Stochastic equation for the state vector

Many quantum information applications are based on the strong-coupling regime in which the relaxation times τ are much longer than the dynamical coupling times T between the subsystems. For two- and three-wave couplings those times are determined by effective Rabi frequencies, $T^{-1} \sim |\Omega_R^{(2,3)}|$. As shown in [19,49], the method of the stochastic equation for the state vector is often the most convenient way to describe the nonperturbative dynamics of open strongly coupled systems; it leads to simpler derivations for the observables and characterization of entanglement than the operator-valued Heisenberg-Langevin equations or the master equation for the density matrix.

Indeed, when applied to strongly coupled systems the Heisenberg approach leads to the nonlinear operator-valued equations even in the simplest case of a single two-level atom coupled to a single-mode field [40]. In contrast, the equations for the state-vector components are always linear; they contain much fewer variables as compared to the density matrix equations and are split into low-dimensional blocks in the RWA, leading to analytic solutions for both two-wave [40] and three-wave [19,49] resonant coupling.

One potential difficulty with this approach is that dissipation and fluctuations may lead to the coupling between different blocks of equations for the state-vector components that were uncoupled in a closed system. However, in the strong-coupling regime the coupling through dissipative reservoirs is weak (scales as a small parameter T/τ) and can be taken into account perturbatively [19,49].

Following [19,49], we apply the stochastic equation for the state vector to derive analytic solution for the parametric coupling of a two-level fermionic quantum emitter to two boson fields. The stochastic equation has the following general form:

$$\frac{d}{dt}|\Psi\rangle = -\frac{i}{\hbar}\hat{H}_{\text{eff}}|\Psi\rangle - \frac{i}{\hbar}|\mathfrak{R}\rangle. \tag{33}$$

Here $|\Psi\rangle$ is the state vector; $|\mathfrak{R}\rangle$ is the noise term satisfying $\overline{|\mathfrak{R}\rangle} = 0$, where the bar means averaging over the noise statistics; $\hat{H}_{\text{eff}} = \hat{H} + \hat{H}^{(\text{ah})}$ is an effective Hamiltonian which is a non-Hermitian operator. Its non-Hermitian component $\hat{H}^{(\text{ah})}$ describes the effects of relaxation. The expressions for $\hat{H}^{(\text{ah})}$ and $|\mathfrak{R}\rangle$ must be consistent with each other to guarantee the conservation of the noise-averaged norm $\overline{\langle\Psi(t)|\Psi(t)\rangle} = 1$, and ensure that the system reaches a physically meaningful steady state in the absence of any external driving force. To calculate the observables from the state vector given by Eq. (33), one should apply a standard procedure but with an important extra step: averaging over the noise statistics, i.e., $q = \overline{\langle\Psi|\hat{q}|\Psi\rangle}$, where $\hat{q}$ is a quantum-mechanical operator corresponding to the observable q.

Perhaps the most popular version of the stochastic approach to derive the state vector, i.e., the stochastic Schrödinger equation (SSE), is its application for numerical Monte Carlo simulations within the method of quantum jumps [40–48]. The stochastic equation in a different form, the Schrödinger-Langevin equation (SLE), was suggested to describe the Brownian motion of a quantum particle in a constant field [62,63]. Generally, using some version of the stochastic equation fits within the narrative of the Langevin method [64]. Within the Langevin approach which describes the system with stochastic equations of evolution, the averaging over the reservoir degrees of freedom is equivalent to averaging over the statistics of the noise sources [65]. This paradigm allows one to describe open systems without relying on the density matrix.

B. Comparison with the Lindblad formalism

It was shown in [19] that one can choose the form of $\hat{H}^{(\text{ah})}$ and $|\mathfrak{R}\rangle$ in such a way that the observables calculated with Eq. (33) will coincide with those obtained by solving the master equation in the Lindblad approximation. The corresponding master equation has the form [40]

$$\frac{d}{dt}\hat{\rho} = -\frac{i}{\hbar}[\hat{H}, \hat{\rho}] + \hat{L}(\hat{\rho}), \tag{34}$$

where $\hat{L}(\hat{\rho})$ is the relaxation operator (Lindbladian) which can be represented as

$$\hat{L}(\hat{\rho}) = -\frac{i}{\hbar}\left(\hat{H}^{(\text{ah})}\hat{\rho} - \hat{\rho}\hat{H}^{(\text{ah})\dagger}\right) + \delta\hat{L}(\hat{\rho}). \tag{35}$$

The equivalence (in the above sense) between the stochastic equation and the Lindblad approach exists if we substitute the anti-Hermitian part of the Hamiltonian from Eq. (35) into Eq. (33), and postulate the following correlation properties for the noise source:

$$\overline{|\mathfrak{R}(t')\rangle\langle\mathfrak{R}(t'')|} = \hbar^2\delta(t'-t'')\delta\hat{L}(\hat{\rho})_{\hat{\rho}\Longrightarrow\overline{|\Psi\rangle\langle\Psi|}}. \tag{36}$$

C. Parametric decay of the electron excitation into a photon and a phonon

We will describe the dynamics near the three-wave electron-photon-phonon resonance by the stochastic Eq. (33) with the parametric Hamiltonian Eq. (11). We will seek the state vector in the form

$$\Psi = \sum_{n,\alpha=0}^{\infty,\infty}\left(C_{\alpha n0}|\alpha\rangle|n\rangle|0\rangle + C_{\alpha n1}|\alpha\rangle|n\rangle|1\rangle\right),$$

where the order of indices corresponds to

$$C_{\text{phonon photon fermion}}|\text{phonon}\rangle|\text{photon}\rangle|\text{fermion}\rangle.$$

Consider the initial state with an excited electron and no bosonic excitations, of the type $|\Psi(0)\rangle = |0\rangle|0\rangle|1\rangle$. Near the resonance $\omega_e \approx \omega + \Omega$ the three-wave coupling leads to the excitation of the state $|1\rangle|1\rangle|0\rangle$. In the zero-temperature limit, which is valid when the reservoir temperature is much lower than the transition frequency (for optical frequencies it is satisfied even at room temperature), relaxation processes could populate only the states with lower energies: $|0\rangle|1\rangle|0\rangle$, $|1\rangle|0\rangle|0\rangle$, and $|0\rangle|0\rangle|0\rangle$. Therefore, for this initial condition the state vector will have five components:

$$|\Psi(t)\rangle = C_{000}(t)|0\rangle|0\rangle|0\rangle + C_{010}(t)|0\rangle|1\rangle|0\rangle + C_{100}(t)|1\rangle|0\rangle|0\rangle + C_{110}(t)|1\rangle|1\rangle|0\rangle + C_{001}(t)|0\rangle|0\rangle|1\rangle. \quad (37)$$

Note that we are not restricting the basis in any way and only considering the initial conditions leading to single-photon and -phonon states to simplify algebra: see, for example, the Appendix in [50] where arbitrary multiphoton states are considered in the same way, leading of course to more cumbersome expressions. Another reason to consider such initial conditions is that single-photon states are used in most applications, whereas generating multiphoton Fock states remains a major challenge.

To determine the anti-Hermitian part $\hat{H}^{(\mathrm{ah})}$ of the Hamiltonian which describes relaxation and the correlator $\overline{|\Re(t')\rangle\langle\Re(t'')|}$ describing fluctuations, we will use the expression for the total Lindbladian of the system including a two-level "atom," photons, and phonons [40]. For simplicity we will assume zero temperature of dissipative reservoirs, which is satisfied at $T \ll \hbar\omega$. The finite-temperature expressions are given in [19,49]. Then the Lindbladian is

$$L(\hat{\rho}) = L_e(\hat{\rho}) + L_{em}(\hat{\rho}) + L_p(\hat{\rho}), \quad (38)$$

$$L_e(\hat{\rho}) = -\frac{\gamma}{2}(\hat{\sigma}^\dagger\hat{\sigma}\hat{\rho} + \hat{\rho}\hat{\sigma}^\dagger\hat{\sigma} - 2\hat{\sigma}\hat{\rho}\hat{\sigma}^\dagger), \quad (39)$$

$$L_{em}(\hat{\rho}) = -\frac{\mu_\omega}{2}(\hat{c}^\dagger\hat{c}\hat{\rho} + \hat{\rho}\hat{c}\hat{c}^\dagger - 2\hat{c}\hat{\rho}\hat{c}^\dagger), \quad (40)$$

$$L_p(\hat{\rho}) = -\frac{\mu_\Omega}{2}(\hat{b}^\dagger\hat{b}\hat{\rho} + \hat{\rho}\hat{b}\hat{b}^\dagger - 2\hat{b}\hat{\rho}\hat{b}^\dagger), \quad (41)$$

where γ, μ_ω, and μ_Ω are relaxation rates of corresponding subsystems.

Then the stochastic equation for the state vector takes the form

$$\begin{pmatrix} \frac{d}{dt} & 0 & 0 \\ 0 & \frac{d}{dt} + i\omega_{010} + \gamma_{010} & 0 \\ 0 & 0 & \frac{d}{dt} + i\omega_{100} + \gamma_{100} \end{pmatrix} \begin{pmatrix} C_{000} \\ C_{010} \\ C_{100} \end{pmatrix} = -\frac{i}{\hbar}\begin{pmatrix} \Re_{000} \\ \Re_{010} \\ \Re_{100} \end{pmatrix}, \quad (42)$$

$$\begin{pmatrix} \frac{d}{dt} + i\omega_{110} + \gamma_{110} & i\Omega_R^{(3)*} \\ i\Omega_R^{(3)} & \frac{d}{dt} + i\omega_{001} + \gamma_{001} \end{pmatrix} \begin{pmatrix} C_{110} \\ C_{001} \end{pmatrix} = -\frac{i}{\hbar}\begin{pmatrix} \Re_{110} \\ \Re_{001} \end{pmatrix}, \quad (43)$$

where

$$\Re_{\alpha ni} = \langle \alpha ni|\Re\rangle;$$

$$\omega_{010} = \omega,\ \omega_{100} = \Omega,\ \omega_{110} = \omega + \Omega,\ \omega_{001} = \omega_e;$$

$$\gamma_{010} = \tfrac{1}{2}\mu_\omega,\ \gamma_{100} = \tfrac{1}{2}\mu_\Omega,\ \gamma_{110} = \tfrac{1}{2}(\mu_\omega + \mu_\Omega),\ \gamma_{001} = \tfrac{1}{2}\gamma.$$

The correlators of the noise sources in Eqs. (42) and (43) are

$$\overline{\Re^*_{\alpha ni}(t')\Re_{\beta mj}(t'')} = \hbar^2 D_{\alpha ni,\beta mj}(t')\delta(t' - t''), \quad (44)$$

where the quantities $D_{\alpha ni,\beta mj}$ are determined using Eqs. (36) and (38)–(41). For the diagonal elements of the correlators we obtain

$$\begin{aligned} D_{110,110} &= D_{001,001} = 0, \\ D_{100,100} &= \mu_\omega\overline{|C_{110}|^2}, \\ D_{010,010} &= \mu_\Omega\overline{|C_{110}|^2}, \\ D_{000,000} &= \gamma\overline{|C_{001}|^2} + \mu_\omega\overline{|C_{010}|^2} + \mu_\Omega\overline{|C_{100}|^2}. \end{aligned} \quad (45)$$

The off-diagonal elements are given by

$$\begin{aligned} D_{\alpha ni,\beta mj} &= D^*_{\beta mj,\alpha ni}, \\ D_{110,\alpha ni} &= D_{001,\alpha ni} = D_{100,010} = 0, \\ D_{000,100} &= \mu_\omega\overline{C^*_{010}C_{110}}, \\ D_{000,010} &= \mu_\Omega\overline{C^*_{100}C_{110}}. \end{aligned} \quad (46)$$

The dependence of quantities $D_{\alpha ni,\beta mj}$ in the right-hand side of Eq. (44) on time t' is due to the time dependence of amplitudes $C_{\alpha ni}$ which enter Eqs. (45) and (46). The derivation of the stochastic equation for the state vector including pure dephasing processes and the finite temperature of the reservoirs has been discussed in [19,49].

Equations (43) describe the dynamic generation of an entangled state of the type $|MIX\rangle = A(t)|0\rangle|0\rangle|1\rangle + B(t)|1\rangle|1\rangle|0\rangle$ whereas Eqs. (42) describe the relaxation dynamics leading to relaxation of populations to states with lower energies. The quantities $D_{010,010}$ and $D_{100,100}$ in Eqs. (45) are associated with processes of the relaxation to states $|0\rangle|1\rangle|0\rangle$ and $|1\rangle|0\rangle|0\rangle$ from the entangled state $|MIX\rangle$. The structure of the expression for $D_{000,000}$ corresponds to the relaxation of the system from the entangled state to the ground state via both "direct" pathway $|0\rangle|0\rangle|1\rangle \to |0\rangle|0\rangle|0\rangle$ and multistep pathways $|1\rangle|1\rangle|0\rangle \to |0\rangle|1\rangle|0\rangle \to |0\rangle|0\rangle|0\rangle$ and $|1\rangle|1\rangle|0\rangle \to |1\rangle|0\rangle|0\rangle \to |0\rangle|0\rangle|0\rangle$, as illustrated in Figs. 3 and 5 below.

D. Expressions for noise sources in the stochastic equation

In addition to the expressions for noise correlators, it is convenient to know more detailed expressions for the random functions describing the noise sources $\Re_{\alpha ni}(t)$. The effect of the reservoir on the dynamic system is characterized by the matrix elements of the operator which determines coupling to the reservoir. For a weak coupling these matrix elements are linear with respect to the matrix elements of the operators describing the dynamical system. Therefore, the functions $\Re_{\alpha ni}(t)$ should depend linearly on the components of the state vector of the system.

Here we again consider the low-temperature case when the relaxation processes can bring the populations only down, not

up. When the reservoirs for each subsystem are statistically independent, one can try the following ansatz:

$$\Re_{\alpha ni}(t) = \hbar\sqrt{\gamma}C_{\alpha n(i+1)}(t)f_e(t) + \hbar\sqrt{\mu_\omega}C_{\alpha(n+1)i}(t)f_{em}(t) + \hbar\sqrt{\mu_\Omega}C_{(\alpha+1)ni}(t)f_p(t), \quad (47)$$

where $\overline{f_{e,em,p}} = 0$. Here $f_{e,em,p}(t)$ are random functions that are determined by the statistics of noise in unperturbed electron, photon, and phonon reservoirs. The functions $f_{e,em,p}$ should not depend on the set of variables $C_{\alpha ni}$ within the above approximations.

The linear dependence of the noise term on the state vector was also assumed in SLE [62,63], in which the noise terms had the form

$$|\Re\rangle = \hat{U}(\mathbf{r}, t)|\Psi\rangle, \quad (48)$$

where $\hat{U}(\mathbf{r}, t)$ is the fluctuating component of the potential.

To ensure that Eq. (47) leads to the correlators Eq. (44)–(46) that are consistent with the Lindblad master equation, one needs first to define the correlators of the random functions in Eq. (47) in the following way:

$$\overline{f_\kappa^*(t')f_\lambda(t'')} = \delta_{\kappa\lambda}\delta(t' - t''), \quad (49)$$

where $\kappa, \lambda = e, em, p$, i.e., the fluctuations in different reservoirs are independent and Markovian. Second, one has to assume that the correlations are factorized when calculating the averages

$$\overline{C_{\alpha ni}^*(t')C_{\beta mj}(t'')f_\kappa^*(t')f_\lambda(t'')} = \overline{C_{\alpha ni}^*(t')C_{\beta mj}(t'')}\ \overline{f_\kappa^*(t')f_\lambda(t'')}. \quad (50)$$

Equation (49) looks obvious, whereas the factorization in Eq. (50) is valid only in linear approximation with respect to relaxation constants γ and $\mu_{\omega,\Omega}$. However, the Lindbladian of the form given in Eqs. (38)–(41) is itself valid within the same approximation. Therefore, Eqs. (47), (49), and (50) lead to all expressions in Eqs. (45) and (46). One also has to keep in mind that with our choice of our initial conditions the amplitudes $C_{\alpha ni} = 0$ for all states with energies above those in states $|1\rangle|1\rangle|0\rangle$ and $|0\rangle|0\rangle|1\rangle$.

V. DYNAMICS OF ENTANGLED FERMION-PHOTON-PHONON STATES IN A DISSIPATIVE SYSTEM

Here we write an explicit solution of Eqs. (42) and (43) for the initial state vector $|\Psi(0)\rangle = |0\rangle|0\rangle|1\rangle$, when $C_{001}(0) = 1$, $C_{000}(0) = C_{010}(0) = C_{100}(0) = C_{110}(0) = 0$. Assuming exact resonance at $\omega_e = \omega + \Omega$, and omitting intermediate steps described in Appendix A, we obtain the solution for the five-component state vector:

$$|\Psi\rangle = e^{-i\omega_e t}e^{-\frac{\gamma_{110}+\gamma_{001}}{2}t}\left\{\left[\cos(\tilde{\Omega}_R t) + \frac{\gamma_{110} - \gamma_{001}}{2\tilde{\Omega}_R}\sin(\tilde{\Omega}_R t)\right]|0\rangle|0\rangle|1\rangle + ie^{-i\theta}\sin(\tilde{\Omega}_R t)|1\rangle|1\rangle|0\rangle\right\} + \delta C_{001}|0\rangle|0\rangle|1\rangle + \delta C_{110}|1\rangle|1\rangle|0\rangle + C_{000}|0\rangle|0\rangle|0\rangle + C_{100}|1\rangle|0\rangle|0\rangle + C_{010}|0\rangle|1\rangle|0\rangle, \quad (51)$$

where

$$\overline{\delta C_{001}} = \overline{\delta C_{110}} = \overline{C_{000}} = \overline{C_{100}} = \overline{C_{010}} = 0, \quad (52)$$

$$\overline{|\delta C_{001}|^2} = \overline{|\delta C_{110}|^2} = 0. \quad (53)$$

Here the effective Rabi frequency $\tilde{\Omega}_R = \sqrt{|\Omega_R^{(3)}|^2 - \frac{(\gamma_{110}-\gamma_{001})^2}{4}}$ and $\theta = \mathrm{Arg}[\Omega_R^{(3)}]$.

It follows from Eq. (51) that in the entangled state $|MIX\rangle = A(t)|0\rangle|0\rangle|1\rangle + B(t)|1\rangle|1\rangle|0\rangle$ the amplitudes $A(t)$ and $B(t)$ oscillate at the effective Rabi frequency and decay with the decay rate

$$\gamma_{MIX} = \frac{\gamma_{110} + \gamma_{001}}{2} = \frac{1}{4}(\mu_\omega + \mu_\Omega + \gamma). \quad (54)$$

The occupation probabilities $|C_{001}|^2$ and $|C_{110}|^2$ are plotted in Fig. 2 as a function of normalized time $\tilde{\Omega}_R t$, along with the real parts of their eigenfrequencies obtained from Eqs. (43) as a function of detuning from the nonlinear resonance $\omega + \Omega - \omega_e$. Although the plots look like standard anticrossing behavior and decaying Rabi oscillations, one should keep in mind that (1) the anticrossing occurs not at the standard exciton-photon or phonon-photon resonance, but at the nonlinear resonance, which is controlled by the nonlinear coupling strength $\Omega_R^{(3)}$ and entangles three degrees of freedom; (2) the relaxation rates of each individual subsystem enter the analytic expressions plotted in Fig. 2 and the decay rate of an entangled state in a nontrivial way, as is obvious from Eq. (54). The presented solution provides the way to retrieve the analytic dependence of any observable on the relaxation and coupling parameters and determine correctly the criterion for observing the strong parametric coupling and entanglement in frequency or time domain. Two obvious examples for such observables are photon and phonon emission spectra that are derived and plotted in Sec. VI (see Figs. 4 and 6).

The expressions for the occupation probabilities $\overline{|C_{100}|^2}$, $\overline{|C_{010}|^2}$, and $\overline{|C_{000}|^2}$ that are valid under the condition $\tilde{\Omega}_R \gg \gamma_{ani}$ are presented in Appendix A.

VI. EMISSION SPECTRA OF PHOTONS AND PHONONS FROM THE PARAMETRIC DECAY OF THE ELECTRON EXCITATION

A. Derivation of the emission spectra from the solution of the stochastic equation for the state vector: A general scheme

Consider for definiteness the EM radiation out of a cavity. Its power spectrum received by the detector is given by [40,66]

$$P(\nu) = AS(\nu),$$

where

$$S(\nu) = \frac{1}{\pi}\mathrm{Re}\int_0^\infty d\tau\, e^{i\nu\tau}\int_0^\infty dt\, K(t, \tau), \quad (55)$$

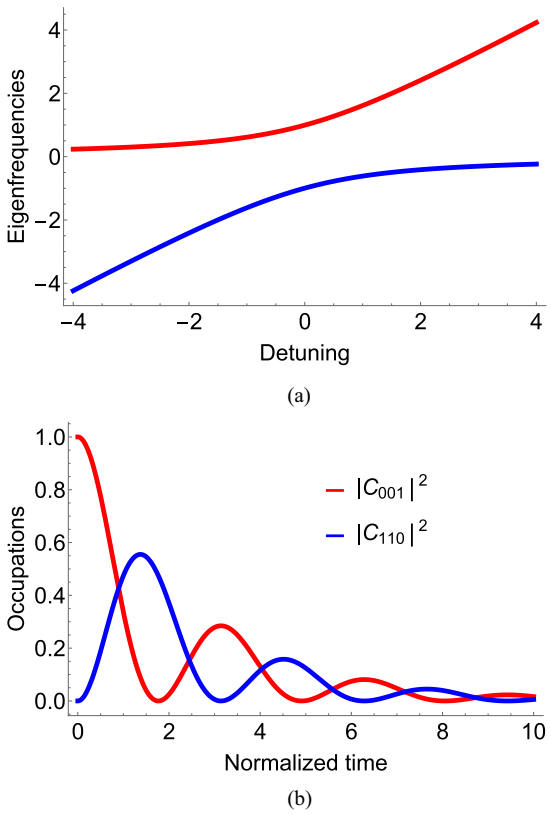

FIG. 2. (a) Real parts of eigenstate frequencies of Eqs. (43), shifted by the electron transition frequency ω_e and normalized by $|\Omega_R^{(3)}|$, as a function of detuning from the nonlinear resonance $\omega + \Omega - \omega_e$ normalized by $|\Omega_R^{(3)}|$. The relaxation rates are $\mu_\omega = \mu_\Omega = 0.3|\Omega_R^{(3)}|$ and $\gamma = 0.2|\Omega_R^{(3)}|$. (b) Occupation probabilities $|C_{001}|^2$ and $|C_{110}|^2$ from Eqs. (A2) and (A3) as a function of normalized time $\tilde{\Omega}_R t$ for the same relaxation rates.

$K = \langle \hat{c}^\dagger(t)\hat{c}(t+\tau)\rangle$, $\langle \dots \rangle$ is a quantum-mechanical averaging. The coefficient A includes the Q factor of a cavity, spatial structure of the outgoing field, and the position and properties of the detector.

To calculate the power spectrum one needs to know the solution of the Heisenberg-Langevin equations for the field operators $\hat{c}(t)$ and $\hat{c}^\dagger(t)$, then calculate the correlator, and average it over the statistics of Langevin noise: $K \Rightarrow \overline{\langle \hat{c}^\dagger(t)\hat{c}(t+\tau)\rangle}$. However, as we already discussed, the Heisenberg-Langevin equations become nonlinear in the strong-coupling regime. Therefore, it may be more convenient to obtain the spectra from the solution of the stochastic Eq. (33) for the state vector. The general procedure is as follows.

First, we need to transform the correlator

$$K(t,\tau) = \langle \hat{c}^\dagger(t)\hat{c}(t+\tau)\rangle = \langle \Psi(0)|\hat{c}^\dagger(t)\hat{c}(t+\tau)|\Psi(0)\rangle \tag{56}$$

to the Schrödinger picture without taking into account dissipation and fluctuations. If $\hat{U}(t)$ is the unitary operator of evolution of the system, one can write

$$\begin{aligned} K &= \langle \Psi(0)|\hat{U}^\dagger(t)\hat{c}^\dagger\,\hat{U}(t)\hat{U}^\dagger(t+\tau)\hat{c}\,\hat{U}(t+\tau)|\Psi(0)\rangle \\ &= \langle \hat{c}\,\Psi(t)|\hat{U}(t)\hat{U}^\dagger(t+\tau)|\hat{c}\,\Psi(t+\tau)\rangle, \end{aligned} \tag{57}$$

where $\hat{c}$ is the Schrödinger's (constant) operator which we will treat as an initial condition for the Heisenberg operator $\hat{c}(t)$ at $t = 0$. We will use the notation $\hat{U}(t) \equiv \hat{U}_{t_0}(t')$, where we indicate explicitly the initial moment of time t_0 and the duration of evolution $t' = t - t_0$. This will lead to the following replacements in Eq. (57): $\hat{U}(t) \Longrightarrow \hat{U}_0(t)$, $\hat{U}(t+\tau) \Longrightarrow \hat{U}_0(t+\tau)$. Furthermore, we obviously have

$$\hat{U}_0(t+\tau) = \hat{U}_t(\tau)\hat{U}_0(t) \tag{58}$$

which gives

$$\begin{aligned} K &= \langle \hat{c}\,\Psi(t)|\hat{U}_0(t)(\hat{U}_t(\tau)\hat{U}_0(t))^\dagger|\hat{c}\,\Psi(t+\tau)\rangle \\ &= \langle \hat{c}\,\Psi(t)|\hat{U}_0(t)\hat{U}_0^\dagger(t)\hat{U}_t^\dagger(\tau)|\hat{c}\,\Psi(t+\tau)\rangle. \end{aligned}$$

Taking into account $\hat{U}_0(t')\hat{U}_0^\dagger(t') = 1$, we obtain

$$K = \langle \hat{U}_t(\tau)\hat{c}\,\Psi(t)\,|\hat{c}\,\Psi(t+\tau)\rangle. \tag{59}$$

Second, introducing the notations

$$\Psi_{\hat{C}}(t) = \hat{c}\,\Psi(t),\ \Phi(t,\tau) = \hat{U}_t(\tau)\Psi_{\hat{C}}(t), \tag{60}$$

we arrive at

$$K(t,\tau) = \langle \Phi(t,\tau)\,|\Psi_{\hat{C}}(t+\tau)\rangle. \tag{61}$$

Therefore, in order to calculate the correlator K through the solution of the equation for the state vector, one has to perform the following steps:

(a) Find vector $|\Psi_{\hat{C}}(t+\tau)\rangle = \hat{c}\Psi(t+\tau)$, where $\Psi(t+\tau)$ is the solution for the state vector $|\Psi\rangle$ at the time interval $[0, t+\tau]$ with initial condition $|\Psi(0)\rangle$.

(b) Find vector $|\Phi(t,\tau)\rangle$. To do that, one has to solve for the state vector $|\Psi\rangle$ at the time interval $[t, t+\tau]$ with initial condition $|\Psi_{\hat{C}}(t)\rangle$. The vector $|\Psi_{\hat{C}}(t)\rangle$ is the same as in part (a), but instead of the time interval $[0, t+\tau]$ one has to take the time interval $[0, t]$.

To check Eq. (61) for consistency, we note that in the absence of dissipation one can go back from this equation to the standard expression which follows directly from the initial Eq. (56):

$$K(t,\tau) = \langle \Psi(0)|e^{i\frac{\hat{H}}{\hbar}t}\hat{c}^\dagger e^{i\frac{\hat{H}}{\hbar}\tau}\hat{c}e^{-i\frac{\hat{H}}{\hbar}(t+\tau)}|\Psi(0)\rangle.$$

If the dynamic system is open, then a complete closed system "the dynamic system + reservoir" has its own unitary operator of evolution $\hat{U}_{t_0}(t')$. Therefore, Eq. (61) should be valid for a complete system as well which includes the reservoir variables. Now we apply the Langevin method which assumes that the averaging over the statistics of noise sources entering a stochastic equation [in this case Eq. (33)] is equivalent to averaging over the reservoir variables. Therefore, we can solve Eq. (33) and, following the above steps, find the functions $\Psi_{\hat{C}}(t)$, $\Psi_{\hat{C}}(t+\tau)$, and $\Phi(t,\tau)$ which are now dependent on the noise sources. Then we substitute the latter two functions into Eq. (61) and perform averaging over the noise statistics. As a result, we obtain

$$K(t,\tau) = \overline{\langle\, \Phi(t,\tau)\,|\Psi_{\hat{C}}(t+\tau)\rangle}. \tag{62}$$

B. Photon emission spectra for the parametric decay of an excited electron

Here we apply the general recipe of calculating $K(t,\tau)$ formulated in the previous section to a particular example of the

parametric decay of an initially excited fermionic two-level system under strong coupling to a nonlinear electron-photon-phonon resonance. In [19] we used a simplified model to analyze the fermion-photon-phonon entanglement, in which all relaxation pathways to the ground state $|0\rangle|0\rangle|0\rangle$ are assumed to be "direct," which corresponds to taking all correlators equal to zero except $D_{000,000}$. This approach is essentially the Weisskopf-Wigner method, modified in order to conserve the norm of the state vector. It gives a correct result for the decay rate γ_{MIX} of the entangled state. At the same time, including multistep decay pathways changes the spectra qualitatively and is of principal importance when interpreting the emission spectra.

Omitting intermediate derivation steps outlined in Appendix B, we obtain

$$S(\nu) = \frac{1}{\pi}\mathrm{Re}\int_0^\infty d\tau\, e^{i\nu\tau}\int_0^\infty dt\, K(t,\tau) = S_1(\nu) + S_2(\nu) + S_3(\nu), \tag{63}$$

where

$$S_1(\nu) = \frac{2\tilde{\Omega}_R^2}{\pi\Gamma\left(4\tilde{\Omega}_R^2+\Gamma^2\right)}\mathrm{Re}\frac{\Gamma+\frac{\mu_\Omega}{2}-i(\nu-\omega)}{[\gamma_{\rm ac}-i(\nu-\omega)]^2+\tilde{\Omega}_R^2},$$
$$S_2(\nu) = \frac{\tilde{\Omega}_R^2}{\pi\Gamma\left(4\tilde{\Omega}_R^2+\Gamma^2\right)}\frac{\mu_\Omega}{\frac{\mu_\omega^2}{4}+(\nu-\omega)^2}, \tag{64}$$
$$S_3(\nu) = \frac{\mu_\Omega\tilde{\Omega}_R^2}{\pi\Gamma(\gamma_d^2+\tilde{\Omega}_R^2)(4\tilde{\Omega}_R^2+\Gamma^2)} \times\left\{-\mathrm{Re}\frac{\Gamma_d[\gamma_{\rm ac}-i(\nu-\omega)]+2\tilde{\Omega}_R^2-\gamma_d\Gamma}{[\gamma_{\rm ac}-i(\nu-\omega)]^2+\tilde{\Omega}_R^2} + \frac{\Gamma_d\frac{\mu_\omega}{2}}{\frac{\mu_\omega^2}{4}+(\nu-\omega)^2}\right\}.$$

The parameters Γ, $\gamma_{\rm ac}$, γ_d, and Γ_d are expressed through the relaxation rates of the electron, photon, and phonon subsystems μ_ω, μ_Ω, and γ as

$$\Gamma = \gamma_{110}+\gamma_{001} = \frac{1}{2}(\mu_\omega+\mu_\Omega+\gamma),\ \gamma_{\rm ac} = \gamma_{100}+\frac{\Gamma}{2} = \frac{1}{4}(\mu_\omega+\gamma)+\frac{3}{4}\mu_\Omega,$$
$$\gamma_d = \gamma_{100}+\frac{\Gamma}{2}-\gamma_{010} = \frac{1}{4}(\gamma-\mu_\omega)+\frac{3}{4}\mu_\Omega,\ \Gamma_d = \Gamma+2\gamma_d = 2\mu_\Omega+\gamma.$$

The expression for the power spectrum $S(\nu)$ contains three terms $S_{1,2,3}$. The term $S_3(\nu)$ consists of two terms which have the same spectral shapes as the functions $S_1(\nu)$ and $S_2(\nu)$, respectively. Therefore, including the term $S_3(\nu)$ in Eq. (63) leads only to corrections to the amplitudes of the functions $S_{1,2}(\nu)$; moreover, under the strong-coupling conditions $\tilde{\Omega}_R \gg \gamma_{ani}$ these corrections are small: of the order of $\sim\frac{\mu_\Omega(\Gamma+\gamma_{\rm ac})}{\tilde{\Omega}_R^2}$ for the function $S_1(\nu)$ and of the order of $\sim\frac{\Gamma_d\mu_\omega}{\tilde{\Omega}_R^2}$ for the function $S_2(\nu)$. For qualitative discussion we will neglect the contribution of $S_3(\nu)$ and keep only the terms $S_1(\nu)$ and $S_2(\nu)$, although all terms are included in the spectra plotted in Fig. 4.

Figure 3 indicates all transitions that give contributions to the photon emission. The function $S_1(\nu)$ describes the emission spectrum at the transition $|1\rangle|1\rangle|0\rangle \to |1\rangle|0\rangle|0\rangle$, which is split due to Rabi oscillations. The width of the peaks located at frequencies $\nu = \omega\pm\tilde{\Omega}_R$ is equal to $\gamma_{\rm ac} = \frac{\mu_\Omega}{2}+\frac{\Gamma}{2}$. Here $\frac{\Gamma}{2} = \frac{1}{4}(\mu_\omega+\mu_\Omega+\gamma) = \gamma_{MIX}$ is the decay rate of the entangled state $|MIX\rangle = A(t)|0\rangle|0\rangle|1\rangle + B(t)|1\rangle|1\rangle|0\rangle$ [see Eq. (51)], and $\frac{\mu_\Omega}{2}$ is the broadening of the state $|1\rangle|0\rangle|0\rangle$ due to relaxation. The spectrum given by $S_1(\nu)$ agrees with the one obtained in [19].

The function $S_2(\nu)$ describes the emission due to a two-step relaxation process described in Sec. IV C: $|1\rangle|1\rangle|0\rangle \to |0\rangle|1\rangle|0\rangle \to |0\rangle|0\rangle|0\rangle$. The photons are emitted at the transition $|0\rangle|1\rangle|0\rangle \to |0\rangle|0\rangle|0\rangle$, which is not affected by Rabi oscillations; see Fig. 3. Therefore, this contribution has a standard Lorentzian shape of an emitter at frequency ω:

$$S_2(\nu) \propto \frac{1}{\gamma_{010}^2+(\nu-\omega)^2} = \frac{1}{\frac{\mu_\omega^2}{4}+(\nu-\omega)^2}.$$

In the strong-coupling regime $\tilde{\Omega}_R \gg \gamma_{ani}$ the ratio of the amplitude of this central peak at frequency $\nu=\omega$ to the amplitudes of the split peaks at frequencies $\nu = \omega\pm\tilde{\Omega}_R$ is given by

$$\frac{S_2(\omega)}{S_1(\omega\pm\tilde{\Omega}_R)} \approx \frac{\mu_\Omega(\mu_\omega+\gamma+3\mu_\Omega)}{\mu_\omega^2}. \tag{65}$$

When $\mu_\Omega \to 0$, Eq. (65) gives $\frac{S_2(\omega)}{S_1(\omega\pm\tilde{\Omega}_R)} \to 0$: indeed without phonon relaxation the state $|0\rangle|1\rangle|0\rangle$ cannot be populated from $|1\rangle|1\rangle|0\rangle$; therefore, the two-step radiation channel is suppressed. In the opposite limit of a fast phonon relaxation, when $\mu_\Omega \gg \mu_\omega, \gamma$, we obtain $\frac{S_2(\omega)}{S_1(\omega\pm\tilde{\Omega}_R)} \gg 1$, i.e., the

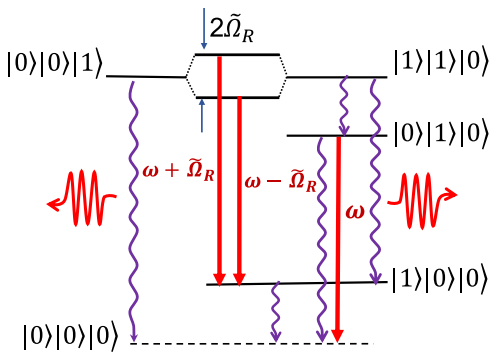

FIG. 3. Energy levels of |phonon⟩|photon⟩|electron⟩ states involved into the photon emission in the parametric decay of a single-electron excitation in a coupled phonon-photon-electron system. Bold red arrows indicate photon emission transitions with their peak frequencies labeled. Wavy purple arrows indicate various relaxation pathways.

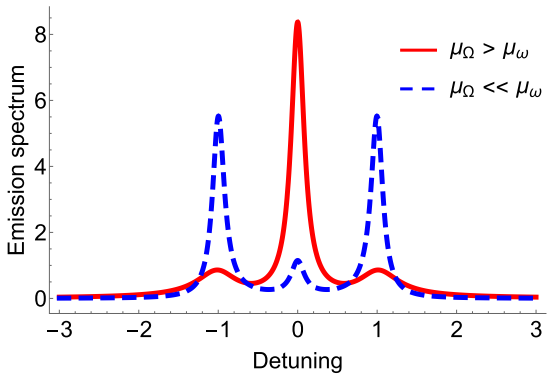

FIG. 4. Normalized photon emission spectra $\tilde{\Omega}_R^2 S(\nu)$ as a function of normalized detuning $\frac{\nu-\omega}{\tilde{\Omega}_R}$ from the cavity-mode frequency ω, for two different values of the phonon relaxation rate: $\mu_\Omega = 0.3$ (red solid line) and $\mu_\Omega = 0.02$ (blue dashed line). Other relaxation rates are $\mu_\omega = 0.2$ and $\gamma = 0.1$. All relaxation constants are in units of $\tilde{\Omega}_R$.

side peaks are weaker and more broadened than the central peak. The latter statement is true despite the large Rabi frequency $\tilde{\Omega}_R \gg \mu_\Omega$. Indeed, when $\tilde{\Omega}_R \gg \mu_\Omega$ the interaction has the time to mix the states $|1\rangle|1\rangle|0\rangle$ and $|0\rangle|0\rangle|1\rangle$ before the phonon relaxation kicks in. Nevertheless, if $\mu_\Omega \gg \mu_\omega, \gamma$ the phonon relaxation is able to transfer population to state $|0\rangle|1\rangle|0\rangle$ faster than the radiative transition $|1\rangle|1\rangle|0\rangle \to |1\rangle|0\rangle|0\rangle$ corresponding to the Rabi-split spectrum.

This behavior is illustrated in Fig. 4 which shows photon emission spectra given by Eqs. (63) and (64) as a function of frequency detuning $\nu - \omega$ from the cavity-mode resonance, for two different values of the phonon relaxation rate: $\mu_\Omega = 1.5\mu_\omega$ (red solid line) and $\mu_\Omega = 0.1\mu_\omega$ (blue dashed line). The electron relaxation rate is kept at $\gamma = 0.1$ and its exact value is not important for the overall shape of the spectra, although it affects absolute values and widths of the peaks. All quantities are normalized by $\tilde{\Omega}_R$.

The relative magnitudes of the peaks and their widths depend sensitively on different combinations of the relaxation rates $\gamma, \mu_\omega, \mu_\Omega$. The onset of the strong-coupling regime in the frequency domain is determined by the visibility of nonlinear Rabi splitting between the side peaks in Fig. 4, i.e., the condition $\tilde{\Omega}_R > \frac{\gamma_{ac}}{2}$. We point out again that the relaxation rates of the individual subsystems enter the quantum dynamics in a very nontrivial way, and one needs to know all of them to evaluate the feasibility of strong coupling in any particular system. The reverse is also true: once the strong-coupling regime is reached, measurements of the photoluminescence spectra yield both the relaxation rates and the nonlinear coupling strength in the system.

A more detailed discussion of the feasibility of strong coupling at the nonlinear resonance in particular systems can be found in [19]. Here we only point out that in dielectric microcavities the photon relaxation rates can be very low, in the μeV range, and the strong-coupling threshold is likely to be determined by relaxation of the electron or vibrational transitions. In plasmonic nanocavities the photon relaxation rate can easily be tens of meV and will likely dominate the strong-coupling threshold. On the other hand, the nonlinear coupling strength $\Omega_R^{(3)}$ is much higher in plasmonic nanocavities because of greatly enhanced electric field localization and electric field gradient. One can obtain the magnitude of $\Omega_R^{(3)}$ of the order of 100 meV for the field localization in the few nm range, which is now routinely demonstrated in plasmonic nanocavities.

C. Phonon emission spectra

There is a complete symmetry for the two bosonic fields in the decay process close to the nonlinear resonance $\omega_e = \omega + \Omega$. Therefore, we can obtain the phonon emission spectrum from the expressions for the photon emission spectrum Eqs. (63) and (64), after replacing

$$\omega \Longleftrightarrow \Omega, \ \mu_\omega \Longleftrightarrow \mu_\Omega, \ \gamma_{010} \Longleftrightarrow \gamma_{100}.$$

This results in

$$S_p(\nu) = S_{1p}(\nu) + S_{2p}(\nu) + S_{3p}(\nu), \tag{66}$$

where

$$\begin{aligned}
S_{1p}(\nu) &= \frac{2\tilde{\Omega}_R^2}{\pi\Gamma\left(4\tilde{\Omega}_R^2 + \Gamma^2\right)} \mathrm{Re} \frac{\Gamma + \frac{\mu_\Omega}{2} - i(\nu - \Omega)}{[\tilde{\gamma}_{\rm ac} - i(\nu - \Omega)]^2 + \tilde{\Omega}_R^2}, \\
S_{2p}(\nu) &= \frac{\tilde{\Omega}_R^2}{\pi\Gamma\left(4\tilde{\Omega}_R^2 + \Gamma^2\right)} \frac{\mu_\omega}{\frac{\mu_\Omega^2}{4} + (\nu - \Omega)^2}, \\
S_{3p}(\nu) &= \frac{\mu_\omega \tilde{\Omega}_R^2}{\pi\Gamma\left(\tilde{\gamma}_d^2 + \tilde{\Omega}_R^2\right)\left(4\tilde{\Omega}_R^2 + \Gamma^2\right)} \left\{ -\mathrm{Re} \frac{\tilde{\Gamma}_d[\tilde{\gamma}_{\rm ac} - i(\nu - \Omega)] + 2\tilde{\Omega}_R^2 - \tilde{\gamma}_d\Gamma}{[\tilde{\gamma}_{\rm ac} - i(\nu - \Omega)]^2 + \tilde{\Omega}_R^2} + \frac{\tilde{\Gamma}_d \frac{\mu_\Omega}{2}}{\frac{\mu_\Omega^2}{4} + (\nu - \Omega)^2} \right\}, \\
\tilde{\gamma}_{\rm ac} &= \gamma_{010} + \frac{\Gamma}{2} = \frac{1}{4}(\mu_\Omega + \gamma) + \frac{3}{4}\mu_\omega, \ \tilde{\gamma}_d = \gamma_{010} + \frac{\Gamma}{2} - \gamma_{100} = \frac{1}{4}(\gamma - \mu_\Omega) + \frac{3}{4}\mu_\omega, \\
\tilde{\Gamma}_d &= \Gamma + 2\tilde{\gamma}_d = 2\mu_\omega + \gamma.
\end{aligned} \tag{67}$$

Similarly to the photon spectrum, the term $S_{3p}(\nu)$ is the sum of two terms which have the same spectral shape as $S_{1p}(\nu)$ and $S_{2p}(\nu)$, but much smaller magnitudes if $\tilde{\Omega}_R \gg \gamma_{ani}$. Therefore, we will again include only the first two terms in qualitative discussion, but include all terms when plotting the spectra.

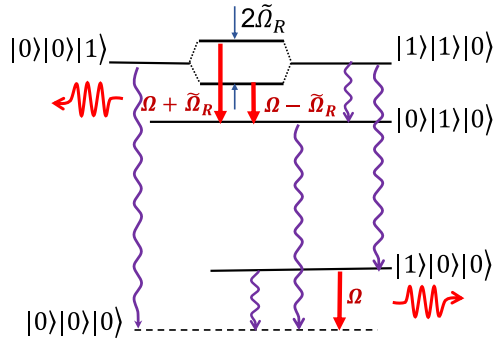

FIG. 5. Energy levels of $|\text{phonon}\rangle|\text{photon}\rangle|\text{electron}\rangle$ states involved into the phonon emission in the parametric decay of a single-electron excitation in a coupled phonon-photon-electron system. Bold red arrows indicate phonon emission transitions with their peak frequencies labeled. Wavy purple arrows indicate various relaxation pathways.

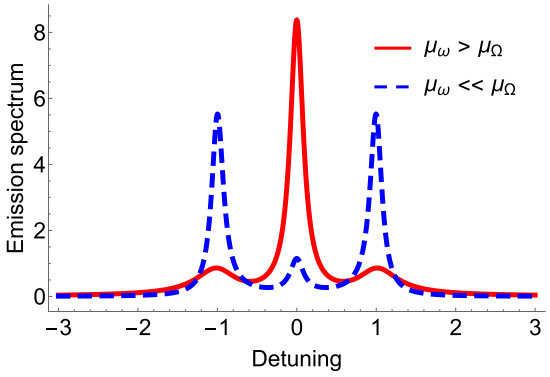

FIG. 6. Normalized phonon emission spectra $\tilde{\Omega}_R^2 S_p(\nu)$ as a function of normalized detuning $\frac{\nu-\Omega}{\tilde{\Omega}_R}$ from the vibrational mode frequency Ω, for two different values of the photon relaxation rate: $\mu_\omega = 0.3$ (red solid line) and $\mu_\omega = 0.02$ (blue dashed line). Other relaxation rates are $\mu_\Omega = 0.2$ and $\gamma = 0.1$. All relaxation constants are in units of $\tilde{\Omega}_R$.

Figure 5 shows all transitions giving contributions to the phonon emission spectrum, with their peak frequencies indicated. The function $S_{1p}(\nu)$ describes the phonon emission spectrum due to the transition $|1\rangle|1\rangle|0\rangle \to |0\rangle|1\rangle|0\rangle$, which demonstrates Rabi splitting. The width of the peaks centered at frequencies $\nu = \Omega \pm \tilde{\Omega}_R$ is equal to $\tilde{\gamma}_{\text{ac}} = \frac{\mu_\omega}{2} + \frac{\Gamma}{2}$. The function $S_{2p}(\nu)$ describes phonon emission due to a two-step relaxation $|1\rangle|1\rangle|0\rangle \to |1\rangle|0\rangle|0\rangle \to |0\rangle|0\rangle|0\rangle$. The phonons are emitted at the second step, i.e., the transition $|1\rangle|0\rangle|0\rangle \to |0\rangle|0\rangle|0\rangle$, which is not affected by Rabi oscillations. Therefore, the spectrum due to this contribution is a standard Lorentzian line, similarly to the case of photons:

$$S_2(\nu) \propto \frac{1}{\gamma_{100}^2 + (\nu-\Omega)^2} = \frac{1}{\frac{\mu_\Omega^2}{4} + (\nu-\Omega)^2}.$$

The ratio of the amplitude of the central peak at $\nu = \Omega$ to those of the side peaks at frequencies $\nu = \Omega \pm \tilde{\Omega}_R$ at $\tilde{\Omega}_R \gg \gamma_{ani}$ is given by the expression equivalent to Eq. (65) after substituting $\omega \Longleftrightarrow \Omega$ and $\mu_\omega \Longleftrightarrow \mu_\Omega$:

$$\frac{S_{2p}(\Omega)}{S_{1p}(\Omega \pm \tilde{\Omega}_R)} \approx \frac{\mu_\omega(\mu_\Omega + \gamma + 3\mu_\omega)}{\mu_\Omega^2}. \tag{68}$$

The phonon emission spectra are plotted in Fig. 6 as a function of frequency detuning $\nu - \Omega$ from the cavity-mode resonance. This time we keep the phonon relaxation rate fixed at $\mu_\Omega = 0.2$ and plot the spectra for two values of the photon relaxation rate, greater and smaller than μ_Ω: $\mu_\omega = 0.3$ (red solid line) and $\mu_\omega = 0.02$ (blue dashed line). All quantities are normalized by $\tilde{\Omega}_R$. The numbers are chosen to prove the point that the phonon and photon spectra are symmetric with respect to replacement indicated in the beginning of this section.

In experiment, measuring the ratios given by Eqs. (65) and (68) allows one to determine the relationships between all relaxation rates μ_Ω, γ, and μ_ω. Indeed, one can obtain from Eqs. (65) and (68) that

$$\xi_\Omega x^3 + 2x^2 - 2x - \xi_\omega = 0, \; y = \xi_\Omega x^2 - 3 - x,$$

where $x = \frac{\mu_\Omega}{\mu_\omega}$, $y = \frac{\gamma}{\mu_\omega}$, $\xi_\omega = \frac{S_2(\omega)}{S_1(\omega \pm \tilde{\Omega}_R)}$, $\xi_\Omega = \frac{S_{2p}(\Omega)}{S_{1p}(\Omega \pm \tilde{\Omega}_R)}$.

D. Effects of pure dephasing and finite temperature of dissipative reservoirs

Pure dephasing processes do not affect the populations of states with energies below the energy of state $|100\rangle$; see Figs. 3 and 5. Therefore, they will not change the parameters of the central peaks in photon and phonon power spectra in Figs. 4 and 6. At the same time, pure dephasing may affect the dynamics of Rabi oscillations between states $|100\rangle$ and $|110\rangle$. Using the analysis in [19,49,50], one can show that pure dephasing (elastic scattering) can be taken into account by replacing $\frac{\gamma}{2} \longrightarrow \frac{\gamma}{2} + \gamma^{(el)}$ in the equations for the state-vector amplitudes $C_{001,110}$, where $\gamma^{(el)}$ is the inverse scattering time for pure dephasing processes. The same replacement rule for relaxation constants has to be applied in the expressions for the side peaks in photon and phonon emission spectra in Figs. 4 and 6.

It is straightforward to include the effects of finite temperature of dissipative reservoirs; see, e.g., [19] where the general expressions for the relaxation constants and noise correlators are given for arbitrary temperature. However, when the inequalities $\hbar\omega, \hbar\omega_e \gg T$ are satisfied (here T is in energy units), thermal parts of the noise terms have negligible effect on the amplitudes of excited states $C_{001,010,110}$. Therefore, under these conditions one can neglect finite-temperature effects on the dynamics of Rabi oscillations, photon emission spectra, and two side peaks of the phonon spectra. If, in addition, $\hbar\Omega \gg T$, all temperature effects are negligible. When $\hbar\Omega \leqslant T$, finite temperature will enhance the amplitude of the central peak of the phonon spectra due to thermal redistribution of populations between states C_{100} and C_{000}.

VII. CONCLUSIONS

We developed a universal model of strong coupling at three-wave nonlinear resonance which is applicable to a variety of cavity-QED systems with coupled electron, photon, and vibrational degrees of freedom, such as molecular quantum emitters, quantum dots, and cavity optomechanics systems. We obtained the analytic solution for the nonperturbative

quantum dynamics of such systems in the vicinity of the nonlinear resonance, taking into account dissipation and fluctuations for all degrees of freedom in Markov approximation. The presented solution can be used to derive the explicit analytic expression for any observable. As an example, we calculated photon and phonon emission spectra which have a characteristic three-peak form once the strong coupling is reached. We showed how the relative heights and widths of the peaks can be used to extract information about all relaxation rates in the system and the nonlinear coupling strength, or to establish the threshold for reaching the strong-coupling regime.

ACKNOWLEDGMENTS

This work has been supported in part by the Air Force Office for Scientific Research Grant No. FA9550-21-1-0272, National Science Foundation Award No. 1936276, and Texas A&M University through STRP, X-grant, and T3-grant programs. M.T. and M.E. acknowledge the support by the Center of Excellence "Center of Photonics" funded by The Ministry of Science and Higher Education of the Russian Federation, Contract No. 075-15-2020-906.

APPENDIX A: SOLUTION FOR THE STOCHASTIC STATE VECTOR IN THE PRESENCE OF DISSIPATION AND NOISE

1. Derivation of probability amplitudes

The coefficients in the five-component state vector Eq. (51) are given by

$$C_{000}(t) = -\frac{i}{\hbar}\int_0^t \mathfrak{R}_{000}(t')dt',$$
$$C_{010}(t) = -\frac{i}{\hbar}\int_0^t \mathfrak{R}_{010}(t')e^{-i\omega(t-t')-\gamma_{010}(t-t')}dt', \quad \text{(A1)}$$
$$C_{100}(t) = -\frac{i}{\hbar}\int_0^t \mathfrak{R}_{100}(t')e^{-i\Omega(t-t')-\gamma_{100}(t-t')}dt',$$

$$C_{001}(t) = e^{-i\omega_e t}e^{-\frac{\gamma_{110}+\gamma_{001}}{2}t}\left[\cos(\tilde{\Omega}_R t) + \frac{\gamma_{110}-\gamma_{001}}{\tilde{\Omega}_R}\sin(\tilde{\Omega}_R t)\right] + \delta C_{001}, \quad \text{(A2)}$$

$$C_{110}(t) = e^{-i\omega_e t}e^{-\frac{\gamma_{110}+\gamma_{001}}{2}t}(ie^{-i\theta})\sin(\tilde{\Omega}_R t) + \delta C_{110}, \quad \text{(A3)}$$

where the effective Rabi frequency $\tilde{\Omega}_R = \sqrt{|\Omega_R^{(3)}|^2 - \frac{(\gamma_{110}-\gamma_{001})^2}{4}}$, $\theta = \mathrm{Arg}[\Omega_R^{(3)}]$, and the terms $\delta C_{100,110}$ are linear with respect to random functions $\mathfrak{R}_{001}$ and $\mathfrak{R}_{110}$.

The term proportional to $\frac{\gamma_{110}-\gamma_{001}}{\tilde{\Omega}_R}$ in the first of Eqs. (A2) can be omitted when calculating most observables when the dissipation is weak $\tilde{\Omega}_R \gg \gamma_{ani}$ (see, e.g., [19]). However, one has to keep in mind that this term is needed for Eqs. (A2) to satisfy an exact integral of motion of Eqs. (43):

$$\frac{d}{dt}(\overline{|C_{001}|^2} + \overline{|C_{110}|^2}) = -2\gamma_{001}\overline{|C_{001}|^2} - 2\gamma_{110}\overline{|C_{110}|^2}.$$

Note that when averaged over the period $\frac{2\pi}{\tilde{\Omega}_R}$ the integral is conserved even without this term.

2. Derivation of occupation probabilities $|C_{100,010,000}|^2$

A number of correlators of the random functions in Eq. (51) are zero due to Eqs. (45) and (46):

$$\overline{\delta C_{110}^*(t')\mathfrak{R}_{\alpha mi}(t'')} = \overline{\delta C_{001}^*(t')\mathfrak{R}_{\alpha mi}(t'')} = 0, \quad \text{(A4)}$$

$$\overline{\delta C_{001}^*(t')\delta C_{001}(t'')} = \overline{\delta C_{110}^*(t')\delta C_{110}(t'')} = \overline{\delta C_{001}^*(t')\delta C_{110}(t'')} = 0, \quad \text{(A5)}$$

$$\overline{\delta C_{001}^*(t')C_{000}(t'')} = \overline{\delta C_{110}^*(t')C_{100}(t'')} = \overline{\delta C_{001}^*(t')C_{010}(t'')} = \overline{\delta C_{110}^*(t')C_{000}(t'')} = \overline{\delta C_{110}^*(t')C_{100}(t'')} = \overline{\delta C_{110}^*(t')C_{010}(t'')} = 0. \quad \text{(A6)}$$

Equations (A4)–(A6) ensure that the variables δC_{100} and δC_{110} cannot contribute to the values of any observables and therefore can be omitted.

The other correlators are given by the equations that follow from Eqs. (A1):

$$\frac{d}{dt}\overline{C_{100}^* C_{010}} = -(\gamma_{100}+\gamma_{010})\overline{C_{100}^* C_{010}} + D_{100,010},$$
$$\frac{d}{dt}\overline{C_{100}^* C_{000}} = -\gamma_{100}\overline{C_{100}^* C_{000}} + D_{100,000},$$
$$\frac{d}{dt}\overline{C_{010}^* C_{000}} = -\gamma_{010}\overline{C_{010}^* C_{000}} + D_{010,000},$$
$$\frac{d}{dt}\overline{|C_{000}|^2} = D_{000,000},$$
$$\frac{d}{dt}\overline{|C_{010}|^2} = -2\gamma_{010}\overline{|C_{010}|^2} + D_{010,010},$$
$$\frac{d}{dt}\overline{|C_{100}|^2} = -2\gamma_{100}\overline{|C_{100}|^2} + D_{100,100}.$$

Using Eqs. (45) and (46), we arrive at

$$\frac{d}{dt}\overline{C_{100}^* C_{010}} = -\frac{\mu_\omega+\mu_\Omega}{2}\overline{C_{100}^* C_{010}},$$
$$\frac{d}{dt}\overline{C_{100}^* C_{000}} = -\frac{\mu_\Omega}{2}\overline{C_{100}^* C_{000}} + \mu_\omega\overline{C_{110}^* C_{010}}, \quad \text{(A7)}$$
$$\frac{d}{dt}\overline{C_{010}^* C_{000}} = -\frac{\mu_\omega}{2}\overline{C_{010}^* C_{000}} + \mu_\Omega\overline{C_{110}^* C_{100}},$$
$$\frac{d}{dt}\overline{|C_{000}|^2} = \gamma\overline{|C_{001}|^2} + \mu_\omega\overline{|C_{010}|^2} + \mu_\Omega\overline{|C_{100}|^2},$$
$$\frac{d}{dt}\overline{|C_{010}|^2} = -\mu_\omega\overline{|C_{010}|^2} + \mu_\Omega\overline{|C_{110}|^2},$$
$$\frac{d}{dt}\overline{|C_{100}|^2} = -\mu_\Omega\overline{|C_{100}|^2} + \mu_\omega\overline{|C_{110}|^2}. \quad \text{(A8)}$$

Taking into account Eqs. (A6), one can obtain that $\overline{C_{110}^* C_{010}} = \overline{C_{110}^* C_{100}} = 0$ in Eqs. (A7); as a result, for our initial conditions Eqs. (A7) yield

$$\overline{C_{100}^* C_{010}} = \overline{C_{100}^* C_{000}} = \overline{C_{010}^* C_{000}} = 0. \quad \text{(A9)}$$

The last two equations in Eqs. (A8) give

$$\overline{|C_{010}|^2} = \mu_\Omega e^{-\mu_\omega t}\int_0^t e^{\mu_\omega \tau}\overline{|C_{110}|^2}d\tau,$$

$$\overline{|C_{100}|^2} = \mu_\omega e^{-\mu_\Omega t}\int_0^t e^{\mu_\Omega \tau}\overline{|C_{110}|^2}d\tau.$$

Substituting here the function from Eq. (A2) and taking into account Eqs. (A5) and (A6) results in

$$\overline{|C_{100}|^2} = \mu_\omega e^{-\mu_\Omega t}\int_0^t e^{\frac{\mu_\Omega-\mu_\omega-\gamma}{2}\tau}\sin^2(\tilde{\Omega}_R\tau)d\tau,$$

$$\overline{|C_{010}|^2} = \mu_\Omega e^{-\mu_\omega t}\int_0^t e^{\frac{\mu_\omega-\mu_\Omega-\gamma}{2}\tau}\sin^2(\tilde{\Omega}_R\tau)d\tau.$$

For further integration we use the limit $\frac{\gamma_{\alpha ni}}{\tilde{\Omega}_R} \ll 1$, leading to

$$\overline{|C_{100}|^2} \approx \frac{\mu_\omega}{\mu_\Omega-\mu_\omega-\gamma}\left(e^{-\frac{\mu_\Omega+\mu_\omega+\gamma}{2}t}-e^{-\mu_\Omega t}\right), \quad \text{(A10)}$$

$$\overline{|C_{010}|^2} \approx \frac{\mu_\Omega}{\mu_\omega-\mu_\Omega-\gamma}\left(e^{-\frac{\mu_\Omega+\mu_\omega+\gamma}{2}t}-e^{-\mu_\omega t}\right). \quad \text{(A11)}$$

Note that Eqs. (A10) and (A11) do not contain any divergence when $[\pm(\mu_\omega-\mu_\Omega)-\gamma] \longrightarrow 0$. Indeed,

$$\lim_{(\mu_\Omega-\mu_\omega-\gamma)\longrightarrow 0}\left[\frac{e^{-\frac{\mu_\Omega+\mu_\omega+\gamma}{2}t}-e^{-\mu_\Omega t}}{\mu_\Omega-\mu_\omega-\gamma}\right] = \frac{1}{2}te^{-\mu_\Omega t},$$

$$\lim_{(\mu_\omega-\mu_\Omega-\gamma)\longrightarrow 0}\left[\frac{e^{-\frac{\mu_\Omega+\mu_\omega+\gamma}{2}t}-e^{-\mu_\omega t}}{\mu_\omega-\mu_\Omega-\gamma}\right] = \frac{1}{2}te^{-\mu_\omega t}.$$

Now we return to the first of Eqs. (A8), which yields

$$\overline{|C_{000}|^2} = \int_0^t(\gamma\overline{|C_{001}|^2}+\mu_\omega\overline{|C_{010}|^2}+\mu_\Omega\overline{|C_{100}|^2})d\tau.$$

We substitute Eqs. (A10) and (A11) into the second and third terms in the integrand and substitute the expression $\overline{|C_{001}|^2}$ which follows from Eqs. (A2) into the first term in the integrand. Neglecting the small terms $\propto\frac{\gamma_{110}-\gamma_{001}}{\tilde{\Omega}_R}$ and $\frac{\gamma_{\alpha ni}}{\tilde{\Omega}_R}$ the integration results in

$$\overline{|C_{000}|^2} = \frac{\gamma(\gamma-\mu_\Omega-\mu_\omega)}{\gamma^2-(\mu_\Omega-\mu_\omega)^2}\left(1-e^{-\frac{\mu_\Omega+\mu_\omega+\gamma}{2}t}\right) - \left(\mu_\Omega\frac{1-e^{-\mu_\omega t}}{\mu_\omega-\mu_\Omega-\gamma}+\mu_\omega\frac{1-e^{-\mu_\Omega t}}{\mu_\Omega-\mu_\omega-\gamma}\right). \quad \text{(A12)}$$

APPENDIX B: CALCULATION OF EMISSION SPECTRA BASED ON THE STOCHASTIC SCHRÖDINGER EQUATION

Note the following steps. (a) Use the expressions (A1)–(A3) to find the vector $|\Psi(t)\rangle$. (b) Determine vectors $|\Psi_{\hat{C}}(t)\rangle$ and $|\Psi_{\hat{C}}(t+\tau)\rangle$, resulting in

$$|\Psi_{\hat{C}}(t)\rangle = \hat{c}|\Psi(t)\rangle = C_{110}(t)|1\rangle|0\rangle|0\rangle + C_{010}(t)|0\rangle|0\rangle|0\rangle, \quad \text{(B1)}$$

$$|\Psi_{\hat{C}}(t+\tau)\rangle = \hat{c}|\Psi(t+\tau)\rangle = C_{110}(t+\tau)|1\rangle|0\rangle|0\rangle + C_{010}(t+\tau)|0\rangle|0\rangle|0\rangle. \quad \text{(B2)}$$

(c) To determine the vector $|\Phi(t,\tau)\rangle$ we will use the solution of Eqs. (42) and (43) at the time interval $[t, t+\tau]$ where the initial condition $|\Psi_{\hat{C}}(t)\rangle$ is given by Eq. (B1). In our case, Eq. (B1) determines the initial value of the state vector; its subsequent evolution is determined by a simple Eq. (42) for the amplitudes of states $|1\rangle|0\rangle|0\rangle$ and $|0\rangle|0\rangle|0\rangle$. As a result, vector $|\Phi(t,\tau)\rangle$ is given by

$$\begin{aligned}|\Phi(t,\tau)\rangle &= C^{(\Phi)}_{100}(t,\tau)|1\rangle|0\rangle|0\rangle + C^{(\Phi)}_{000}(t,\tau)|0\rangle|0\rangle|0\rangle \\ &= \left(e^{-i\omega\tau-\gamma_{100}\tau}C_{110}(t) - \frac{i}{\hbar}\int_t^{t+\tau}\mathfrak{R}^{(\Phi)}_{100}(t,t')e^{-i\omega(\tau+t-t')-\gamma_{100}(\tau+t-t')}dt'\right)|1\rangle|0\rangle|0\rangle \\ &+\left(C_{010}(t) - \frac{i}{\hbar}\int_t^{t+\tau}\mathfrak{R}^{(\Phi)}_{000}(t,t')dt'\right)|0\rangle|0\rangle|0\rangle, \end{aligned} \quad \text{(B3)}$$

where functions $C_{110}(t)$ and $C_{010}(t)$ are determined by Eqs. (A1) and (A2).

The superscript (Φ) in the terms $\mathfrak{R}_{\alpha ni}$ in Eq. (B3) means that the correlators of these noise terms correspond to the state vector $|\Phi\rangle$. The dependence on the initial time moment t of the evolution in $\mathfrak{R}^{(\Phi)}_{\alpha ni}(t,t')$ takes into account that the correlators of these random functions may depend on the value of t as a parameter because complex amplitudes $C^{(\Phi)}_{\alpha ni}(t,\tau) \equiv C^{(\Phi)}_{\alpha ni}(t,t'-t)$ depend on this parameter.

Next, we substitute the expressions for $C_{110}(t)$, $C_{010}(t)$, $C_{110}(t+\tau)$ determined by Eqs. (A1) and (A2), into Eqs. (B2) and (B3); after that we substitute Eqs. (B2) and (B3) into Eq. (62). In the resulting expression we average over the noise statistics, taking into account that the noise sources are delta correlated. Omitting the terms that become zero after averaging, we obtain

$$\begin{aligned}K(t,\tau) &= e^{-i\omega\tau-(\gamma_{100}+\frac{\gamma_{110}+\gamma_{001}}{2})\tau-(\gamma_{110}+\gamma_{001})t}\sin(\tilde{\Omega}_R t)\sin[\tilde{\Omega}_R(t+\tau)] + e^{-i\omega\tau-\gamma_{010}\tau-2\gamma_{010}t}\int_0^t D_{010,010}(t')e^{2\gamma_{010}t'}dt' \\ &+e^{-i\omega(t+\tau)-\gamma_{010}(t+\tau)-2\gamma_{010}t}\int_t^{t+\tau}\tilde{D}_{000,010}(t,t')e^{(i\omega+\gamma_{010})t'}dt'. \end{aligned} \quad \text{(B4)}$$

Here the quantity $D_{010,010}$ is determined by Eqs. (45):

$$D_{010,010} = 2\gamma_{010}\overline{|C_{110}(t')|^2} = \mu_\Omega\overline{|C_{110}(t')|^2}. \quad \text{(B5)}$$

The function $\tilde{D}_{000,010}(t,t')$ corresponds to the following correlator:

$$\overline{\mathfrak{R}^{(\Phi)*}_{000}(t,t')\mathfrak{R}_{010}(t'')} = \hbar^2\tilde{D}_{000,010}(t,t')\delta(t'-t''). \quad \text{(B6)}$$

To calculate the value of $\tilde{D}_{000,010}(t,t')$ it is not enough to have expressions Eq. (45) and (46) because it is determined by correlations between the noise terms for *different* state vectors $|\Phi\rangle$ and $|\Psi\rangle$, which correspond to the solutions of the equation for the state vector with *different initial conditions*. We need to use the expression for the noise source obtained in Sec. IV D. From Eqs. (47), (49), and (50) we obtain

$$\tilde{D}_{000,010}(t,t') = \mu_\Omega\overline{C^{(\Phi)*}_{100}(t,t'-t)C_{110}(t')}. \quad \text{(B7)}$$

Substituting here the appropriate term from Eq. (B3) gives

$$\tilde{D}_{000,010}(t,t') = e^{i\omega(t'-t)-\gamma_{100}(t'-t)-2\gamma_{010}t}\overline{C^*_{110}(t)C_{110}(t')}. \quad \text{(B8)}$$

Substituting Eqs. (B5) and (B8) into Eq. (B4), we arrive at

$$\begin{aligned}K(t,\tau) = {} & e^{-i\omega\tau-\left(\gamma_{100}+\frac{\Gamma}{2}\right)\tau-\Gamma t}\sin(\tilde{\Omega}_R t)\sin[\tilde{\Omega}_R(t+\tau)] \\ & + e^{-i\omega\tau-\gamma_{010}\tau}\mu_\Omega\left[\frac{2\tilde{\Omega}_R^2}{\gamma_n\left(4\tilde{\Omega}_R^2+\gamma_n^2\right)}e^{-2\gamma_{010}t} - \frac{1}{2\gamma_n}e^{-\Gamma t} - \frac{1}{4(2i\tilde{\Omega}_R-\gamma_n)}e^{2i\tilde{\Omega}_R t-\Gamma t} + \frac{1}{4(2i\tilde{\Omega}_R+\gamma_n)}e^{-2i\tilde{\Omega}_R t-\Gamma t}\right] \\ & + e^{-i\omega\tau-\gamma_{010}\tau-\Gamma t}\frac{\mu_\Omega}{4}\left[\frac{e^{(-\gamma_d+i\tilde{\Omega}_R)\tau}-1}{-\gamma_d+i\tilde{\Omega}_R}(1-e^{2i\tilde{\Omega}_R t}) + \text{c.c.}\right], \end{aligned} \quad \text{(B9)}$$

where we denoted $\Gamma = \gamma_{110}+\gamma_{001}$, $\gamma_n = \Gamma - 2\gamma_{010}$, $\gamma_d = \gamma_{100}+\frac{\Gamma}{2}-\gamma_{010}$. Now we have everything to determine the emission spectra given by Eq. (55). Using the values of $\gamma_{100} = \frac{\mu_\Omega}{2}$, $\gamma_{010} = \frac{\mu_\omega}{2}$, and $\gamma_{001} = \frac{\gamma}{2}$, we arrive at Eq. (63).

[1] M. K. Schmidt, R. Esteban, A. Gonzalez-Tudela, G. Giedke, and J. Aizpurua, Quantum mechanical description of Raman scattering from molecules in plasmonic cavities, ACS Nano **10**, 6291 (2016).

[2] J. del Pino, J. Feist, and F. J. Garcia-Vidal, Signatures of vibrational strong coupling in Raman scattering, J. Phys. Chem. **119**, 29132 (2015).

[3] J. del Pino, F. J. Garcia-Vidal, and J. Feist, Exploiting Vibrational Strong Coupling to Make an Optical Parametric Oscillator Out of a Raman Laser, Phys. Rev. Lett. **117**, 277401 (2016).

[4] S. Ramelow, A. Farsi, Z. Vernon, S. Clemmen, X. Ji, J. E. Sipe, M. Liscidini, M. Lipson, and A. L. Gaeta, Strong Nonlinear Coupling in a Si_3N_4 Ring Resonator, Phys. Rev. Lett. **122**, 153906 (2019).

[5] T. Neuman, J. Aizpurua, and R. Esteban, Quantum theory of surface-enhanced resonant Raman scattering (SERRS) of molecules in strongly coupled plasmon-exciton systems, Nanophotonics **9**, 295 (2020).

[6] F. Ge, X. Han, and J. Xu, Strongly coupled systems for nonlinear optics, Laser Photonics Rev. **15**, 2000514 (2021).

[7] K. Wang, M. Seidel, K. Nagarajan, T. Chervy, C. Genet, and T. Ebbesen, Large optical nonlinearity enhancement under electronic strong coupling, Nat. Commun. **12**, 1486 (2021).

[8] J. Flick, N. Rivera, and P. Narang, Strong light-matter coupling in quantum chemistry and quantum photonics, Nanophotonics **7**, 1479 (2018).

[9] D. Wang, J. Flick, and P. Narang, Light-matter interaction of a molecule in a dissipative cavity from first principles, J. Chem. Phys. **154**, 104109 (2021).

[10] A. V. Zasedatelev, A. V. Baranikov, D. Sannikov, D. Urbonas, F. Scafirimuto, V. Yu. Shishkov, E. S. Andrianov, Y. E. Lozovik, U. Scherf, T. Stoferle, R. F. Mahrt, and P. G. Lagoudakis, Single-photon nonlinearity at room temperature, Nature (London) **597**, 493 (2021).

[11] A. Pscherer, M. Meierhofer, D. Wang, H. Kelkar, D. Martin-Cano, T. Utikal, S. Gotzinger, and V. Sandoghdar, Single-Molecule Vacuum Rabi Splitting: Four-Wave Mixing and Optical Switching at the Single-Photon Level, Phys. Rev. Lett. **127**, 133603 (2021).

[12] S. Hughes, A. Settineri, S. Savasta, and F. Nori, Resonant Raman scattering of single molecules under simultaneous strong cavity coupling and ultrastrong optomechanical coupling in plasmonic resonators: Phonon-dressed polaritons, Phys. Rev. B **104**, 045431 (2021).

[13] T. Neuman and J. Aizpurua, Origin of the asymmetric light emission from molecular exciton-polaritons, Optica **5**, 1247 (2018).

[14] J. A. Cwik, P. Kirton, S. De Liberato, and J. Keeling, Excitonic spectral features in strongly coupled organic polaritons, Phys. Rev. A **93**, 033840 (2016).

[15] J. del Pino, J. Feist, and F. J. Garcia-Vidal, Quantum theory of collective strong coupling of molecular vibrationswith a microcavity mode, New J. Phys. **17**, 053040 (2015).

[16] F. Benz, M. K. Schmidt, A. Dreismann, R. Chikkaraddy, Y. Zhang, A. Demetriadou, C. Carnegie, H. Ohadi, B. de Nijs, R. Esteban, J. Aizpurua, and J. J. Baumberg, Single-molecule optomechanics in picocavities, Science **354**, 726 (2016).

[17] K.-D. Park, E. A. Muller, V. Kravtsov, P. M. Sass, J. Dreyer, J. M. Atkin, and M. B. Raschke, Variable-temperature tip-enhanced Raman spectroscopy of single-molecule fluctuations and dynamics, Nano Lett. **16**, 479 (2016).

[18] R. Chikkaraddy, B. de Nijs, F. Benz, S. J. Barrow, O. A. Scherman, E. Rosta, A. Demetriadou, P. Fox, O. Hess, and J. J. Baumberg, Single-molecule strong coupling at room temperature in plasmonic nanocavities, Nature (London) **535**, 127 (2016).

[19] M. Tokman, M. Erukhimova, Y. Wang, Q. Chen, and A. Belyanin, Generation and dynamics of entangled

fermion-photon-phonon states in nanocavities, Nanophotonics **10**, 491 (2021).
[20] C. K. Law, Interaction between a moving mirror and radiation pressure: A Hamiltonian formulation, Phys. Rev. A **51**, 2537 (1995).
[21] S. Mancini, V. I. Manko, and P. Tombesi, Ponderomotive control of quantum macroscopic coherence, Phys. Rev. A **55**, 3042 (1997).
[22] M. Aspelmeyer, T. J. Kippenberg, and F. Marquardt, Cavity optomechanics, Rev. Mod. Phys. **86**, 1391 (2014).
[23] P. Meystre, A short walk through quantum optomechanics, Ann. Phys. **525**, 215 (2013).
[24] P. Roelli, C. Galland, N. Piro, and T. J. Kippenberg, Molecular cavity optomechanics as a theory of plasmon-enhanced Raman scattering, Nat. Nanotechnol. **11**, 164 (2016).
[25] J.-M. Pirkkalainen, S. U. Cho, F. Massel, J. Tuorila, T. T. Heikkila, P. J. Hakonen, and M. A. Sillanpaa, Cavity optomechanics mediated by a quantum two-level system, Nat. Commun. **6**, 6981 (2015).
[26] Y. Chu, P. Kharel, W. H. Renninger, L. D. Burkhart, L. Frunzio, P. T. Rakich, and R. J. Schoelkopf, Quantum acoustics with superconducting qubits, Science **358**, 199 (2017).
[27] S. Hong, R. Riedinger, I. Marinkovic, A. Wallucks, S. G. Hofer, R. A. Norte, M. Aspelmeyer, and S. Groblacher, Hanbury Brown and Twiss interferometry of single phonons from an optomechanical resonator, Science **358**, 203 (2017).
[28] P. Arrangoiz-Arriola, E. A. Wollack, Z. Wang, M. Pechal, W. Jiang, T. P. McKenna, J. D. Witmer, R. Van Laer, and A. H. Safavi-Naeini, Resolving the energy levels of a nanomechanical oscillator, Nature (London) **571**, 537 (2019).
[29] Q. Liao, Y. Ye, P. Lin, N. Zhou, and W. Nie, Tripartite entanglement in an atom-cavity-optomechanical system, Int. J. Theor. Phys. **57**, 1319 (2018).
[30] K. J. Satzinger, Y. P. Zhong, H. Chang, G. A. Peairs, A. Bienfait, M.-H. Chou, A. Y. Cleland, C. R. Conner, E. Dumur, J. Grebel *et al.*, Quantum control of surface acoustic-wave phonons, Nature (London) **563**, 661 (2018).
[31] A. Bienfait, Y. P. Zhong, H.-S. Chang, M.-H. Chou, C. R. Conner, E. Dumur, J. Grebel, G. A. Peairs, R. G. Povey, K. J. Satzinger, and A. N. Cleland, Quantum Erasure Using Entangled Surface Acoustic Phonons, Phys. Rev. X **10**, 021055 (2020).
[32] U. Delic, M. Reisenbauer, K. Dare, D. Grass, V. Vuletic, N. Kiesel, and M. Aspelmeyer, Cooling of a levitated nanoparticle to the motional quantum ground state, Science **367**, 892 (2020).
[33] I. Wilson-Rae and A. Imamoglu, Quantum dot cavity-QED in the presence of strong electron-phonon interactions, Phys. Rev. B **65**, 235311 (2002).
[34] S. Weiler, A. Ulhaq, S. M. Ulrich, D. Richter, M. Jetter, P. Michler, C. Roy, and S. Hughes, Phonon-assisted incoherent excitation of a quantum dot and its emission properties, Phys. Rev. B **86**, 241304(R) (2012).
[35] K. Roy-Choudhury and S. Hughes, Quantum theory of the emission spectrum from quantum dots coupled to structured photonic reservoirs and acoustic phonons, Phys. Rev. B **92**, 205406 (2015).
[36] P. Kaer and J. Mork, Decoherence in semiconductor cavity QED systems due to phonon couplings, Phys. Rev. B **90**, 035312 (2014).
[37] E. V. Denning, M. Bundgaard-Nielsen, and J. Mork, Optical signatures of electron-phonon decoupling due to strong light-matter interactions, Phys. Rev. B **102**, 235303 (2020).
[38] C. Couteau, Spontaneous parametric down-conversion, Contemp. Phys. **59**, 291 (2018).
[39] P. Zoller and C. W. Gardiner, in *Quantum Noise in Quantum Optics: the Stochastic Schrödinger Equation*, Lecture Notes for the Les Houches Summer School LXIII on Quantum Fluctuations, July 1995, edited by E. Giacobino and S. Reynaud (Elsevier, Amsterdam, 1997).
[40] M. O. Scully and M. S. Zubairy, *Quantum Optics* (Cambridge University Press, Cambridge, 1997).
[41] M. B. Plenio and P. L. Knight, The quantum-jump approach to dissipative dynamics in quantum optics, Rev. Mod. Phys. **70**, 101 (1998)
[42] N. Gisin and I. C. Percival, The quantum-state diffusion model applied to open systems, J. Phys. A: Math. Gen. **25**, 5677 (1992).
[43] L. Diosi, N. Gisin, and W. T. Strunz, Non-Markovian quantum state diffusion, Phys. Rev. A **58**, 1699 (1998).
[44] C. Cohen-Tannoudji, B. Zambon, and E. Arimondo, Quantum-jump approach to dissipative processes: application to amplification without inversion, J. Opt. Soc. Am. B **10**, 2107 (1993).
[45] K. Mølmer, Y. Castin, and J. Dalibard, Monte Carlo wave-function method in quantum optics, J. Opt. Soc. Am. B **10**, 524 (1993).
[46] N. Gisin and I. C. Percival, Wave-function approach to dissipative processes: are there quantum jumps?, Phys. Lett. A **167**, 315 (1992).
[47] H. De Raedt, F. Jin, M. I. Katsnelson, and K. Michielsen, Relaxation, thermalization, and Markovian dynamics of two spins coupled to a spin bath, Phys. Rev. E **96**, 053306 (2017).
[48] F. Nathan and M. S. Rudner, Universal Lindblad equation for open quantum systems, Phys. Rev. B **102**, 115109 (2020).
[49] Q. Chen, Y. Wang, S. Almutairi, M. Erukhimova, M. Tokman, and A. Belyanin, Dynamics and control of entangled electron-photon states in nanophotonic systems with time-variable parameters, Phys. Rev. A **103**, 013708 (2021).
[50] M. Tokman, Q. Chen, M. Erukhimova, Y. Wang, and A. Belyanin, Quantum dynamics of open many-qubit systems strongly coupled to a quantized electromagnetic field in dissipative cavities, arXiv:2105.14674.
[51] M. Tokman, Y. Wang, I. Oladyshkin, A. R. Kutayiah, and A. Belyanin, Laser-driven parametric instability and generation of entangled photon-plasmon states in graphene, Phys. Rev. B **93**, 235422 (2016).
[52] M. Tokman, X. Yao, and A. Belyanin, Generation of Entangled Photons in Graphene in a Strong Magnetic Field, Phys. Rev. Lett. **110**, 077404 (2013).
[53] M. D. Tokman, M. A. Erukhimova, and V. V. Vdovin, The features of a quantum description of radiation in an optically dense medium, Ann. Phys. **360**, 571 (2015).
[54] M. Tokman, Z. Long, S. AlMutairi, Y. Wang, M. Belkin, and A. Belyanin, Enhancement of the spontaneous emission in sub-wavelength quasi-two-dimensional waveguides and resonators, Phys. Rev. A **97**, 043801 (2018).
[55] F. Herrera, and F. C. Spano, Absorption and photoluminescence in organic cavity QED, Phys. Rev. A **95**, 053867 (2017).

[56] E. T. Jaynes and F. W. Cummings, Comparison of quantum and semiclassical radiation theories with application to the beam maser, Proc. IEEE **51**, 89 (1963).

[57] M. Tokman, Y. Wang, Q. Chen, L. Shterengas, and A. Belyanin, Generation of entangled photons via parametric down-conversion of lasing modes in semiconductor lasers and waveguides, Phys. Rev. A **105**, 033707 (2022).

[58] V. May and O. Kuhn, *Charge and Energy Transfer Dynamics in Molecular Systems* (Wiley, Weinheim, Germany, 2011).

[59] N. Wu, J. Feist, and F. J. Garcia-Vidal, When polarons meet polaritons: Exciton-vibration interactions in organic molecules strongly coupled to confined light fields, Phys. Rev. B **94**, 195409 (2016).

[60] F. Herrera and F. C. Spano, Cavity-Controlled Chemistry in Molecular Ensembles, Phys. Rev. Lett. **116**, 238301 (2016).

[61] M. A. Zeb, P. G. Kirton, and J. Keeling, Exact states and spectra of vibrationally dressed polaritons, ACS Photonics **5**, 249 (2018).

[62] M. D. Kostin, On the Schrödinger-Langevin equation, J. Chem. Phys. **57**, 3589 (1972).

[63] R. Katz and P. B. Gossiaux, The Schrödinger–Langevin equation with and without thermal fluctuations, Ann. Phys. **368**, 267 (2016).

[64] D. F. Walls and G. J. Milburn, *Quantum Optics* (Springer, Berlin, 1994).

[65] L. D. Landau and E. M. Lifshitz, *Statistical Physics*, Part 1 (Pergamon, Oxford, 1965).

[66] K. H. Madsen and P. Lodahl, Quantitative analysis of quantum dot dynamics and emission spectra in cavity quantum electrodynamics, New J. Phys. **15**, 025013 (2013).